A structural model for the viscoelastic behavior of arterial walls: Continuum formulation and finite element analysis

G.A. Holzapfel*, T.C. Gasser, M. Stadler

Graz University of Technology
Institute for Structural Analysis – Computational Biomechanics
Schiesstattgasse 14-B, A–8010 Graz, Austria
http://www.cis.tu-graz.ac.at/biomech

Appeared in
European Journal of Mechanics A-Solids
Vol. 21 (2002) 441-463

Contents

*Corresponding author. *E-mail address:* gh@biomech.tu-graz.ac.at (G.A. Holzapfel)

A structural model for the viscoelastic behavior of arterial walls: Continuum formulation and finite element analysis

G.A. Holzapfel*, **T.C. Gasser, M. Stadler**

Graz University of Technology
Institute for Structural Analysis – Computational Biomechanics
Schiesstattgasse 14-B, A–8010 Graz, Austria
http://www.cis.tu-graz.ac.at/biomech

Abstract. *In this paper we present a two-layer structural model suitable for predicting reliably the passive (unstimulated) time-dependent three-dimensional stress and deformation states of healthy young arterial walls under various loading conditions. It extends to the viscoelastic regime a recently developed constitutive framework for the elastic strain response of arterial walls (see* HOLZAPFEL *et al.* [2001]*). The structural model is formulated within the framework of nonlinear continuum mechanics and is well-suited for a finite element implementation. It has the special merit that it is based partly on histological information, thus allowing the material parameters to be associated with the constituents of each mechanically-relevant arterial layer. As one essential ingredient from the histological information the constitutive model requires details of the directional organization of collagen fibers as commonly observed under a microscope. We postulate a fully automatic technique for identifying the orientations of cellular nuclei, these coinciding with the preferred orientations in the tissue. The biological material is assumed to behave incompressibly so that the constitutive function is decomposed locally into volumetric and isochoric parts. This separation turns out to be advantageous in avoiding numerical complications within the finite element analysis of incompressible materials. For the description of the viscoelastic behavior of arterial walls we employ the concept of internal variables. The proposed viscoelastic model admits hysteresis loops that are known to be relatively insensitive to strain rate, an essential mechanical feature of arteries of the muscular type. To enforce incompressibility without numerical difficulties, the finite element treatment adopted is based on a three-field Hu-Washizu variational approach in conjunction with an augmented Lagrangian optimization technique. Two numerical examples are used to demonstrate the reliability and efficiency of the proposed structural model for arterial wall mechanics as a basis for large scale numerical simulations.*

*Corresponding author. *E-mail address:* gh@biomech.tu-graz.ac.at (G.A. Holzapfel)

1 Introduction

A reliable constitutive model for arterial walls is an essential prerequisite for a number of different objectives. For example, an efficient constitutive description of arterial walls is essential for: (i) improved diagnostics and therapeutical procedures that are based on mechanical treatments, such as percutaneous transluminal angioplasty (PTA) or bypass surgery; (ii) optimization of the design of arterial prostheses; (iii) study of mechanical factors that may be important in triggering the onset of aneurysms or atherosclerosis, the major cause of human mortality in the western world; (iv) the description of pulse wave dynamics and the interaction between the heart and the circulatory system; and (v) investigation of changes in the arterial system due to age, disease, hypertension and atherosclerosis, which is of fundamental clinical relevance.

We restrict our attention to *preconditioned* materials for which the typical stress softening effects, which occur during the first few load cycles, are no longer evident. In general, only the mechanical response of preconditioned biological materials is published. Biological materials exhibit a nearly repeatable cyclic behavior; the stress-strain relationship is predictable and the associated hysteresis is relatively *insensitive* to strain rate over several decades (nearly constant damping, independent of frequency). After preconditioning, vessel segments behave either elastically or viscoelastically depending strongly on their physiological function and topographical site. Typical viscoelastic behavior of arteries manifests itself in several ways, including stress relaxation, creep, time-dependent recovery of deformation following load removal and frequency-dependence of strength. For the typical mechanical behavior of arterial walls, their mechanical properties and constitutive equations, and for a list of references the reader is referred to the reviews by, for example, HAYASHI [1993] and HUMPHREY [1995], and to the data book edited by ABÈ *et al.* [1996].

In general, *proximal arteries* are of the 'elastic type' and behave elastically, while *distal arteries* are of the 'muscular type' and do not meet the definition of an elastic continuum. They are characterized on the basis of their pronounced viscoelastic behavior. Consequently, the stress at a typical point of a muscular artery at a given time depends on the strain at that time *and* on the strain history which affects the stress. The stress and strain responses to loading and unloading are considerably different. However, the stress-strain relationship during loading and unloading for each cyclic process is unique.

Another important feature of the passive (unstimulated) mechanical behavior of an artery is that the stress-strain response during both loading and unloading is highly nonlinear. At higher strains (pressures) the artery changes to a significantly stiffer tube. The typical (exponential) stiffening effect originates from the 'recruitment' of the embedded wavy collagen fibrils, which result in a markedly anisotropic mechanical behavior of arteries (see, for example, ROACH & BURTON [1957] and NICHOLS & O'ROURKE [1998], Section 4). The fact that the stress increases much faster than the strain seems common to almost all biological soft tissues and was pointed out early on by WERTHEIM [1847] for human tissues. The early work by PATEL & FRY [1969] considers the arterial wall to be cylindrically orthotropic, an assumption generally accepted and used in the literature.

In addition, the deformation of arteries is volume-preserving within the physiological range of

deformation (CAREW *et al.* [1968]), so that arteries, like all other biological soft tissues, may be regarded as *incompressible* materials. For many years it has also been known that the load-free state of arteries does not coincide with the stress-free state (VAISHNAV & VOSSOUGHI [1983]). In general, a load-free arterial ring contains residual stresses (and significant strains), which are essential to consider in order to predict reliably both the global mechanical response and the stress distribution across arterial walls at the physiological state of deformation (see, for example, CHUONG & FUNG [1986] and HOLZAPFEL *et al.* [2000]). More recent studies on dog carotid arteries, performed by DOBRIN [1999], suggest that arterial media act mechanically as *homogeneous* materials, although they are histologically heterogeneous.

Finally, to conclude the description of the general mechanical characteristics of arterial walls we comment briefly on their typical thermoelastic behavior. Since the early work by ROY [1880-82] it has been known that the thermoelastic properties of arteries differ significantly from the vast majority of other materials. In particular, a piece of artery will *contract* its length under tension when its temperature is raised, which is a similar thermomechanical behavior to that observed for rubber-like materials; see, for example, HOLZAPFEL & SIMO [1996], HOLZAPFEL [2000], Chapter 7, and the references therein.

The mathematical description of arterial walls often uses a linearized relationship between the incremental stresses and strains (some examples are given in the data book edited by ABÈ *et al.* [1996]). The associated incremental elastic moduli are applicable only to that specific state of equilibrium from which the moduli were actually taken (by subjecting a material to a small perturbation about a condition of equilibrium). The incremental approach, inappropriate to describe finite deformations with which we are concerned, is still applied by some authors in order to characterize the mechanical properties of arteries. The viscoelastic behavior of arteries is often based on the concept of *pseudo-elasticity* in which the biological material is treated as one elastic material during loading, and another elastic material during unloading (see, for example, FUNG *et al.* [1979] and FUNG [1980]). The concept of pseudo-elasticity has the advantage that mathematical descriptions of stress-strain-history laws for tissues during specific cyclic loading histories are simple; however, the concept provides only a rough approximation for the description a viscoelastic behavior.

The goal of this paper is to propose a three-dimensional structural model capable of simulating the passive (unstimulated) mechanical behavior of healthy young arterial walls in the large viscoelastic strain regime. What is needed is a realistic, histologically-based model for establishing the free energy and evolution equations in terms of physically *meaningful* material parameters. The model needs to be simple enough in order to be able to determine the various material parameters on the basis of suitable experimental tests. It turns out to be useful to consider the network of elastin and collagen within the *nonlinear* continuum theory of the mechanics of fiber-reinforced composites proposed by SPENCER [1984]. In addition, we aim to capture the typical features of arterial response mentioned above with a special emphasis on viscoelasticity. As a special case (at thermodynamic equilibrium) the structural model replicates (compressible) finite hyperelasticity as recently proposed by HOLZAPFEL *et al.* [2000]. Thermodynamic variables such as the entropy and the temperature are not considered here.

We begin, in Section 2, by giving a brief introduction to arterial histology, and continue by

postulating an automatic technique for identifying the orientations of a large number of nuclei, which we assume to coincide with the preferred orientations in the tissue. This is essential information for the structural model introduced in Section 3. The arterial wall, since assumed healthy and young, is approximated as a two-layer thick-walled tube. The fully three-dimensional anisotropic material description for each arterial layer is based on the multiplicative split of the deformation gradient into volumetric and isochoric parts. The histological information about the artery is incorporated in terms of structural tensors. Instead of modeling the loading and unloading curves by two different laws of elasticity (pseudo-elasticity), so-called internal variables are introduced in order to replicate the dissipative mechanism, the non-recoverable energy, of arteries. For these internal variables, appropriate evolution equations and closed form solutions are provided in the form of convolution integrals. Section 4 deals with the finite element formulation of the proposed arterial model suitable for obtaining 'locking-free' numerical results. A three-field Hu-Washizu variational approach is presented together with an augmented Lagrangian method. In Section 5, two representative numerical examples are used to demonstrate the reliability and efficiency of the proposed structural model and to point out certain characteristic features of arterial deformations. Based on a healthy and young arterial segment some of the peculiar viscous effects are studied under various (static and dynamic) boundary loadings.

2 Arterial histology

This section aims to review briefly the histology of arteries and to describe the mechanical characteristics of the arterial components that provide the main *elastic* and *viscoelastic* contributions to the arterial deformation process. In addition, we describe a fully automatic technique for identifying the orientation of smooth muscle cells, these coinciding with the orientations of collagen fibers. The distribution of preferred (fiber) orientations provide important histological information for the structural model proposed in Section 3.

2.1 A brief review of arterial histology and the mechanical roles of arterial components

Arteries are blood vessels with a wide variety of diameters. They are roughly subdivided into two types: *elastic* and *muscular*. Elastic arteries such as the aorta and the carotid and iliac arteries are located close to the heart (proximal arteries), have relatively large diameters and may be regarded as elastic structures. Muscular arteries (distal arteries) such as femoral, celiac and cerebral arteries are smaller, located at the periphery (more distal) and may be regarded as *viscoelastic* structures. Smaller arteries typically display more pronounced viscoelastic behavior than arteries with large diameters; see, for example, TANAKA & FUNG [1974]. It is generally assumed that the content of smooth muscle cells present in an artery is responsible for its viscosity. For example, according to the study by LEAROYD & TAYLOR [1966], a high viscosity is found in the human femoral artery, and this is attributed to its very large muscle content.

Arterial walls are composed of three distinct concentric layers, the *intima*, the *media* and the *adventitia*. The intima is the innermost layer of the artery and offers negligible mechanical strength in healthy young individuals. However, the mechanical contribution of the intima may become significant for aged arteries *(arteriosclerosis)* (the intima becomes thicker and stiffer). In addition, it is important to note that pathological changes of the intimal components *(atherosclerosis)* are associated with significant alterations in the mechanical properties of arterial walls, differing significantly from those of healthy arteries (LEAROYD & TAYLOR [1966] and LANGEWOUTERS *et al.* [1984]).

In the healthy young individuals on which we focus, only the media (the middle layer) and the adventitia (the outermost layer) are responsible for the strength of the arterial wall and play significant mechanical roles by carrying most of the stresses. At low strains (physiological pressures), it is chiefly the media that determines the wall properties (XIE *et al.* [1995]). The heterogeneous media is a highly organized three-dimensional network of elastin, vascular smooth muscle cells and collagen with extracellular matrix proteoglycans (CLARK & GLAGOV [1985]). However, it behaves mechanically as a homogeneous material (DOBRIN [1999]). Due to the high content of smooth muscle cells, it is the media that is believed to be mainly responsible for the viscoelastic behavior of an arterial segment. The adventitia is composed of elastin and collagen fibers that remain slack until higher levels of strain are reached (WOLINSKY & GLAGOV [1964]). At very high strains the adventitia changes to a stiff 'jacket-like' tube which prevents the artery from overstretching and rupturing (SCHULZE-BAUER *et al.* [2001]). The adventitia is surrounded by loose connective tissue and its thickness depends on the type (elastic or muscular), the physiological function of the blood vessel and its topographical site.

The concentration and arrangement of constituent elements and the associated mechanical properties of arterial walls may depend significantly on the species and the topographical site (see, for example, the early work by ROY [1880-82]). The ratio of collagen to elastin in the aorta increases away from the heart (WOLINSKY & GLAGOV [1967]) and the corresponding tensile responses of circumferential and longitudinal specimens vary along the aortic tree (BERGEL [1961*b*], BERGEL [1961*a*], LEAROYD & TAYLOR [1966] and TANAKA & FUNG [1974] among many others). Elastin behaves like a rubber band and can sustain extremely large strains without rupturing (it fractures at low stresses). The concentrically arranged collagen fibers, which are very stiff proteins, contribute to the strength of arterial walls.

For a more detailed account of the different mechanical characteristics, the structure (distribution and orientation) of the interrelated arterial components, the morphological structure and the overall functioning of the blood vessel the reader is referred to, for example, RHODIN [1980], SILVER *et al.* [1989] and HOLZAPFEL *et al.* [2000], Section 2.

2.2 An automatic technique for identifying preferred orientations in arterial layers

The quantitative knowledge of preferred orientations in arterial layers enhances the understanding of the general mechanical characteristics of arterial walls significantly. It is important to note that realistic structural models rely strongly on this knowledge. Collagen fibers are those

components of arterial walls that render the material properties anisotropic. To describe the anisotropic feature, appropriate geometrical data (fiber angles) are required. They serve as an essential set of input data for numerical models.

2.2.1 Introduction and historical overview

High directional correlations between the long axes of cellular shapes and nuclei of, for example, a stained patch of a media may be studied under a microscope. The very first contribution concerning the directional analysis of smooth muscle cells seems to be attributed to RANVIER [1880]. At a later date, STRONG [1938] used a combination of microdissection and etching technique to show that dissected threads of muscle tissues are helically shaped with constant radius. The author concluded that the helical patterns are also present in muscular arteries and that the media is composed mainly of layered structures of helices.

Quantitative studies regarding (helical) pitch angles were carried out by RHODIN [1962], RHODIN [1967], COPE & ROACH [1975] and CANHAM [1977] for several organisms at different locations. These studies do not support the conclusion of a unified orientation of smooth muscle cells drawn by STRONG [1938]. The non-uniformity of fiber orientations in specimens originating from different organisms and different locations was pointed out by WALMSLEY & CANHAM [1979].

Smooth muscle cells provide active contractile elements of the arterial wall and have long and thin centrally located nuclei (see RHODIN [1967] and SOMLYO & SOMLYO [1968]), which can be stained with hematoxylin in order to reveal the cell (nuclei) orientations (WALMSLEY & CANHAM [1979]).

A number of techniques have been proposed for analyzing the orientation of nuclei: WALMSLEY & CANHAM [1979] used a digitizer to enter manually the coordinates of the nuclei of the human intracranial media into a computer. Thereby, the orientation is described by two angles (in the histological plane and in an orthogonal plane). In addition, PETERS *et al.* [1983] used a graphic tablet to digitize the coordinates of nuclei within the human brain artery. As a reference frame of coordinate axes they embedded a precisely trimmed block together with the vessel segment in paraffin wax. The most thorough study was undertaken by TODD *et al.* [1983], in which shape, position, linear dimensions, volumes and orientation of nuclei within several vessel types of male Wistar rats are determined by means of computer-aided analyses. Sections with $0.5\,(\mu\mathrm{m})$ thickness are produced by an ultramicrotome and then stained and cut again to produce ultrathin sections with 60-$80\,(\mathrm{nm})$ thickness. Hence, the digitized contours of cells are assembled into a three-dimensional model by appropriate software tools. Recent studies concentrate on scattering light techniques (FERDMAN & YANNAS [1993] and BILLIAR & SACKS [1997]) and polarized light microscopy using the birefringent optical property of collagen fibers (FINLAY *et al.* [1998]) in order to obtain information about their architecture.

2.2.2 Automatic technique for identifying preferred orientations.

In this section we postulate an automatic technique for obtaining information about preferred orientations in isolated arterial tissues, and, additionally, the concentration of nuclei. It is im-

portant to note that a realistic structural model relies strongly on this type of histological information.

Since a stained patch reveals the orientations of smooth muscle cells, in particular of the associated nuclei (see Figure 1), it is possible to identify the statistical distributions of nuclei in the patch plane. In particular, we detect nuclei on an algorithmic basis by scanning each line of the histological section (image) consecutively. All connected pixels that make up a nucleus are copied to a stack. The stack is then transferred to a program, which determines the orientation of the shape of the nucleus from its associated second-order moment. To continue, the nucleus so detected is then deleted from the original image, and the procedure starts again at the location where the first pixel of the preceding nucleus was detected.

The above mentioned program starts with the computation of the centroid $\mathbf{x}_{\rm c}$ of a nucleus according to $\mathbf{x}_{\rm c} = \sum_{i=1}^{N} \mathbf{x}_i / N$, where N refers to the total number of pixels making up the nucleus. A representative shape of a nucleus is illustrated in Figure 1. The position vector of a typical pixel i relative to a fixed origin is denoted by $\mathbf{x}_i$ and the components of the vectors $\mathbf{x}_{\rm c}$ and $\mathbf{x}_i$ are $x_{\rm c}, y_{\rm c}$ and x_i, y_i, respectively.

Knowing the centroid of the nucleus we may compute the second-order moment, $\mathbf{D}$ say, i.e.

$$\mathbf{D} = \sum_{i=1}^{N} [(\mathbf{r}_i \cdot \mathbf{r}_i)\mathbf{I} - \mathbf{r}_i \otimes \mathbf{r}_i], \tag{1}$$

where we introduced the definition $\mathbf{r}_i = \mathbf{x}_i - \mathbf{x}_{\rm c}$ of the position vectors $\mathbf{r}_i$, and $\mathbf{I}$ denotes the second-order unit tensor which, in index notation, has the form $(\mathbf{I})_{ij} = \delta_{ij}$ with δ_{ij} being the Kronecker delta. To write eq. (1) in a more convenient *matrix* representation, which is useful for computational purposes, we have

$$[\mathbf{D}] = \sum_{i=1}^{N} \begin{bmatrix} (y_i - y_{\rm c})^2 & -(x_i - x_{\rm c})(y_i - y_{\rm c}) \\ -(x_i - x_{\rm c})(y_i - y_{\rm c}) & (x_i - x_{\rm c})^2 \end{bmatrix}. \tag{2}$$

If we imagine that every pixel, for example, possesses mass, then $\mathbf{D}$ may be seen as the *inertia tensor* relative to a fixed origin. It is a symmetric second-order tensor with components forming the entries of the inertia matrix, denoted by $[\mathbf{D}]$ and expressed through eq. (2). The diagonal components $(x_i - x_{\rm c})^2$, $(y_i - y_{\rm c})^2$ and the off-diagonal components $-(x_i - x_{\rm c})(y_i - y_{\rm c})$ of $[\mathbf{D}]$ are associated with the *moments of inertia* and the *product of inertia*, respectively. Considering the eigenvalue problem for the matrix $[\mathbf{D}]$ we may finally find the eigenvalues (which are the principal moments of inertia) and the associated eigenvectors which define the corresponding principal axes. Hence, the orientation of the nucleus is clearly determined by its principal axes, relative to which the product of inertia is zero. To this end it is immaterial whether only perimeter-pixels or all the pixels making up the nucleus are considered. Subsequently, the (mean) angle that occurs between the collagen fibers and the circumferential direction of the respective arterial layer (media, adventitia) is denoted by φ.

Finally, note that special attention is focused on the type of data stored in a stack. In order to avoid artifacts such as scratches, which may occur in a histological section, or nuclei that are

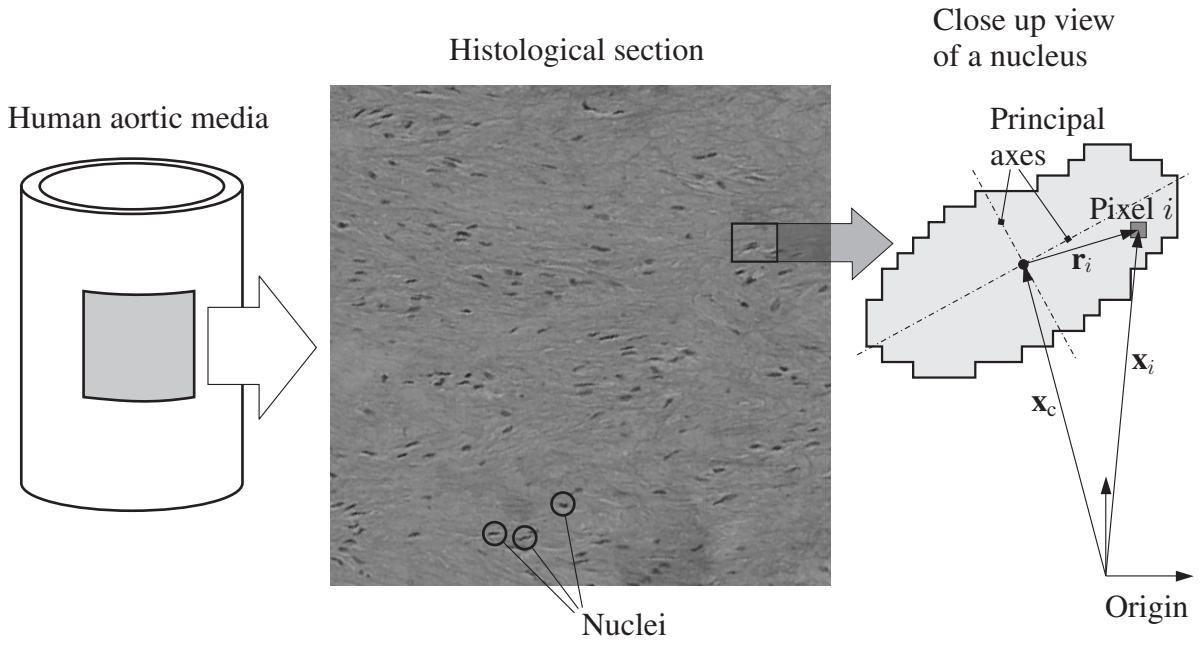

Figure 1: Histological section of a stained patch of a human aortic media. The circumferential orientation of the patch was aligned with the horizontal axis. The algorithm detected 179 nuclei within the image representing a histological size of $0.5 \times 0.5\text{mm}^2$ ($p_{\min} = 15$, $r_{\min} = 2$).

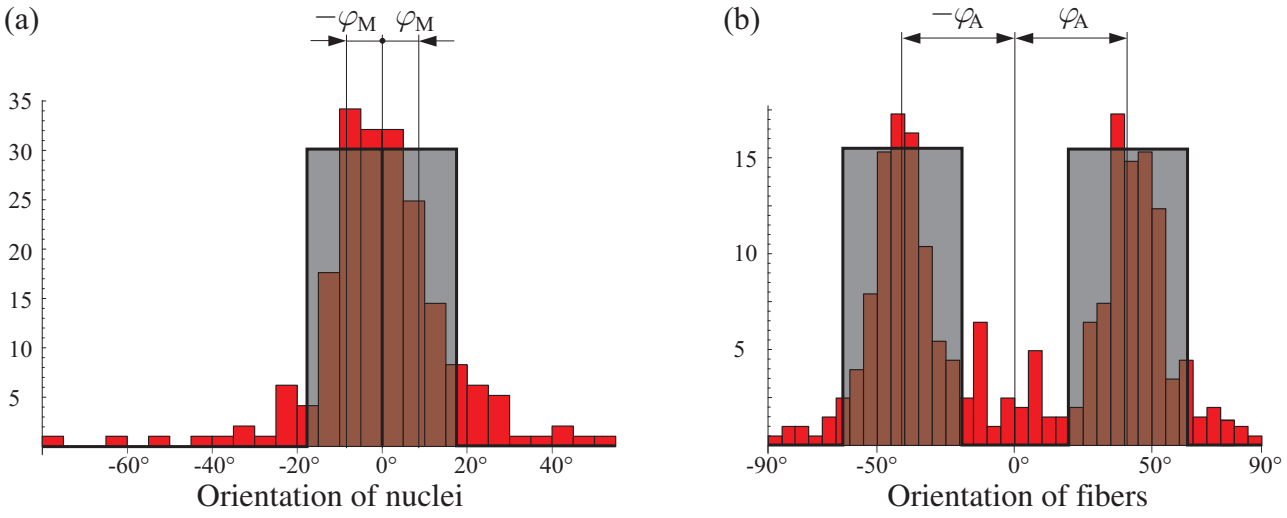

Figure 2: Histograms show statistical distributions of the orientation of nuclei in a human aortic media (a), and of collagen fibers in a human aortic adventita (b). Statistical analyses led to mean angles $\varphi_M = \pm 8.4°$ in the media and $\varphi_A = \pm 41.9°$ in the adventitia.

represented by almost circular shapes, we require (i) a minimum number of pixels $p_{\min}$ that make up a nucleus and (ii) a minimum ratio $r_{\min}$ of larger to smaller eigenvalues (principal moments of inertia). If both criteria are satisfied the nucleus is accepted and its orientation is considered as relevant data.

Example. A histological section of a stained patch of a human aortic *media* with size $0.5 \times 0.5\mathrm{mm}^2$ is considered. The image, as illustrated in Figure 1, was digitized and prepared for scanning by the software tool developed. The horizontal direction of the patch was aligned with the circumferential direction of the vessel. The criteria which ensure that the orientation of a nucleus is considered as relevant data were set to the values $p_{\min} = 15$ and $r_{\min} = 2$.

The algorithm detected 179 nuclei within the image and determined the orientations of all nuclei. A typical statistical distribution of the orientation of nuclei is illustrated in Figure 2(a) in the form of a histogram. The two (light grey) peaks in the figure fill the same area as the histogram. Statistical analyses led to mean angles φ_{M} of the orientations of nuclei (collagen fibers) in the media of $\pm 8.4°$. The result that the collagen fibers in the media are almost circumferentially oriented is in agreement with general histological data of a human aortic media (see, for example, RHODIN [1980]). ■

Figure 2(b) shows the representative results of a statistical analysis performed for a human aortic *adventitia*, which is characterized by predominant orientations of collagen fibers. The mean angles between the collagen fibers and the circumferential direction in the adventitia are, for this sample, determined as $\varphi_{\mathrm{A}} = \pm 41.9°$. The automatic technique for identifying fiber directions in the adventitia is very similar to that described above. Alternatively, for low numbers of nuclei the intra-spatial voids between collagen fiber bundles may be used as indicators for preferred orientations of the tissue.

3 Two-layer structural model for healthy young arterial walls

Healthy young arteries are incompressible, highly deformable composite structures which show nonlinear elastic *and* viscoelastic stress-strain responses with accompanying exponential stiffening effects at higher strains (pressures). The goal of this section is to propose a structural model for the mechanical behavior of arterial walls which considers these major mechanical characteristics and which incorporates histological information. Based on the different mechanical properties and physiological functions of the media and the adventitia we model the healthy young arterial wall as a two-layer fiber-reinforced composite. In order to study stress distributions across the arterial wall the two layers are modeled as thick-walled tubes. Each layer is modeled such that the material parameters involved may be associated with the histological structure of the arterial layer, i.e. collagen and non-collagenous matrix material.

The constitutive model is based on nonlinear continuum mechanics and is formulated so that it is well-suited for numerical realization using the finite element method. It embodies the symmetries of a cylindrically orthotropic material. Since the finite deformation behavior of arterial

walls is regarded as isochoric in nature, and for purposes which become clear within the variational formulation, the constitutive formulation is presented exclusively within the framework of decoupled (volumetric-isochoric) finite viscoelasticity. The subsequent study will be aimed at developing a Lagrangian (material) description of the problem.

3.1 Constitutive framework

3.1.1 Basic kinematics and initial boundary-value problem

Let $\Omega_0 \subset \mathbb{R}^3$ be an open set defining a continuum body (a layer of the artery) with smooth boundary surface $\partial\Omega_0$ positioned in the three-dimensional Euclidean space $\mathbb{R}^3$. We refer to Ω_0 as the reference configuration of the body at (fixed) reference time $t = 0$. The body undergoes a motion $\boldsymbol{\chi}$ during some closed time interval $t \in [0, T]$ of interest. It is expressed via the map $\boldsymbol{\chi} : \tilde{\Omega}_0 \times [0, T] \to \mathbb{R}^3$, where $\tilde{\Omega}_0 = \Omega_0 \cup \partial\Omega_0$ denotes the closure of the open set Ω_0. Now the motion transforms a reference point $\mathbf{X} \in \tilde{\Omega}_0$ into a spatial point $\mathbf{x} = \boldsymbol{\chi}(\mathbf{X}, t)$ for any subsequent (given) time t. Consequently, the motion gives $\boldsymbol{\chi}(\mathbf{X}, t) = \mathbf{X} + \mathbf{u}(\mathbf{X}, t)$, with the displacement field $\mathbf{u}(\mathbf{X}, t)$, and $\mathbf{V}(\mathbf{X}, t) = \partial\boldsymbol{\chi}(\mathbf{X}, t)/\partial t$ is defined to be the Lagrangian description of the velocity field. Furthermore, $\mathbf{F}(\mathbf{X}, t) = \partial\boldsymbol{\chi}(\mathbf{X}, t)/\partial\mathbf{X} = \mathbf{I} + \partial\mathbf{u}/\partial\mathbf{X}$ quantifies the deformation gradient and $J(\mathbf{X}, t) = \det\mathbf{F}$ is the volume change.

Since we have in mind to express the constitutive model in the *Lagrangian description* we introduce the right Cauchy-Green tensor $\mathbf{C}(\mathbf{X}, t) = \mathbf{F}^{\mathrm{T}}\mathbf{F}$ as an appropriate deformation measure. The material time derivative of $\mathbf{C}$ (subsequently denoted by a superimposed dot) is given by $\dot{\mathbf{C}} = 2\mathbf{F}^{\mathrm{T}}\mathbf{d}\mathbf{F}$, where $\mathbf{d}$ is the symmetric part of the spatial velocity gradient $\dot{\mathbf{F}}\mathbf{F}^{-1}$.

We apply now the concept of decoupled (volumetric-isochoric) finite (hyper)elasticity which uses the multiplicative split of the deformation into *volumetric* (dilatational) and *isochoric* (distortional) parts (FLORY [1961], OGDEN [1978]). We write,

$$\mathbf{F} = (J^{1/3}\mathbf{I})\overline{\mathbf{F}}, \qquad \det\overline{\mathbf{F}} \equiv 1\,. \tag{3}$$

With eq. $(3)_1$ and the use of the modified deformation measure $\overline{\mathbf{C}} = \overline{\mathbf{F}}^{\mathrm{T}}\overline{\mathbf{F}}$ the right Cauchy-Green tensor is then given in the form $\mathbf{C} = (J^{2/3}\mathbf{I})\overline{\mathbf{C}}$. The structure of the material at any point $\mathbf{X}$ is characterized by two (second-order) tensors, which we denote by $\mathbf{A}$ and $\mathbf{B}$. The structural tensors provide a measure of the preferred orientations in the different arterial layers.

To describe the history of the deformation, we introduce a set of internal (strain-like) variables, denoted by the second-order tensors $\overline{\boldsymbol{\Gamma}}_\alpha$, $\alpha = 1, \ldots, m$. For the basic idea that we use for the description of inelastic processes, see, for example, VALANIS [1972], LUBLINER [1990], SIMO & HUGHES [1998] or HOLZAPFEL [2000], Section 6.9.

All viscoelasticity is assumed to occur purely by *isochoric* deformations and all *volume changing* deformations are forced to be reversible. Hence, the tensorial (history) variables $\overline{\boldsymbol{\Gamma}}_\alpha$ are akin to $\overline{\mathbf{C}}$. They are not accessible to direct observation, characterize the current departure from equilibrium and contribute to the total strain (stress). The viscoelastic behavior is modeled

by $\alpha = 1, \ldots, m$ viscoelastic processes with corresponding relaxation (or retardation) times $\tau_\alpha \in (0, \infty)$.

The Lagrangian form of Cauchy's first equation of motion has the representation

$$\left.\begin{aligned} \dot{\boldsymbol{\chi}} &= \mathbf{V} \ , \\ \mathrm{Div}(\mathbf{FS}) + \mathbf{b}_0 &= \rho_0 \dot{\mathbf{V}} \, , \end{aligned}\right\} \tag{4}$$

valid for the domain $\Omega_0 \times [0, T]$. In these equations $\mathbf{S} = \mathbf{S}(\mathbf{X}, t)$ is the second Piola-Kirchhoff stress tensor, $\mathbf{b}_0 = \mathbf{b}_0(\mathbf{X}, t)$ is a prescribed (given) reference body force (defined per unit reference volume in Ω_0) that is referred to the reference position $\mathbf{X}$, and $\rho_0(\mathbf{X}) > 0$ is the reference mass density. The term $\rho_0 \dot{\mathbf{V}}$ characterizes the inertia force per unit reference volume. The operator $\mathrm{Div}(\bullet)$ denotes the divergence of a quantity $(\bullet)$ with respect to the reference configuration.

In addition to the differential equations (4) the problem is subject to certain boundary and initial conditions as well. We assume subsequently that the boundary surface $\partial\Omega_0$ is subdivided into a region $\partial\Omega_{0\,\sigma} \subset \partial\Omega_0$ and into a remainder $\partial\Omega_{0\,\mathrm{u}}$, so that these regions, assumed to be time invariant, obey $\partial\Omega = \partial\Omega_{0\,\mathrm{u}} \cup \partial\Omega_{0\,\sigma}$ and $\partial\Omega_{0\,\mathrm{u}} \cap \partial\Omega_{0\,\sigma} = \emptyset$. The required boundary and initial conditions are summarized as

$$\left.\begin{aligned} \mathbf{u}(\mathbf{X}, t) = \overline{\mathbf{u}} \quad &\text{on} \quad \partial\Omega_{0\,\mathrm{u}}, \text{ for all } t \in [0, T], \\ [\mathbf{F}(\mathbf{X}, t)\mathbf{S}(\mathbf{X}, t)]\,\mathbf{N} = \overline{\mathbf{T}} \quad &\text{on} \quad \partial\Omega_{0\,\sigma}, \text{ for all } t \in [0, T], \\ \mathbf{u}(\mathbf{X}, t)|_{t=0} = \mathbf{u}_0 \quad &\text{on} \quad \tilde{\Omega}_0, \\ \mathbf{V}(\mathbf{X}, t)|_{t=0} = \mathbf{V}_0 \quad &\text{on} \quad \tilde{\Omega}_0, \end{aligned}\right\} \tag{5}$$

where the overbars $(\overline{\bullet})$ denote prescribed (given) functions on the boundaries $\partial\Omega_{0\,(\bullet)} \subset \partial\Omega_0$ of the body occupying Ω_0 ($\overline{\mathbf{u}} : \partial\Omega_{0\,\mathrm{u}} \times [0, T] \to \mathbb{R}^3$ for a displacement field and $\overline{\mathbf{T}} : \partial\Omega_{0\,\sigma} \times [0, T] \to \mathbb{R}^3$ for a first Piola-Kirchhoff traction vector, i.e. force measured per unit reference surface area), and $(\bullet)_0$ denote prescribed functions on $\tilde{\Omega}_0$ ($\mathbf{u}_0 : \tilde{\Omega}_0 \to \mathbb{R}^3$ for an initial displacement field and $\mathbf{V}_0 : \tilde{\Omega}_0 \to \mathbb{R}^3$ for an initial velocity field). The prescribed traction vector $\overline{\mathbf{T}}$ in $(5)_2$ corresponds to 'dead' loading (the load does not depend on the motion of the body). The unit exterior vector normal to $\partial\Omega_{0\,\sigma}$ is denoted by $\mathbf{N}$.

The set (4), (5) of equations defines the *strong form* of the initial boundary-value problem. In the following we consider only the *quasi-static* case for which $\rho_0 \dot{\mathbf{V}} = \mathbf{o}$. Additionally we neglect body forces ($\mathbf{b}_0 = \mathbf{o}$). All that remains is to specify a constitutive equation for the stress. This is done in the next section.

3.1.2 Constitutive equations and internal dissipation

In order to derive constitutive equations for isothermal processes (i.e. at constant temperature), we define a Helmholtz free-energy function Ψ (defined per unit reference volume), which describes the viscoelastic deformation of a material point from the reference configuration Ω_0 to some current configuration Ω. For numerical purposes we consider the material as (slightly)

compressible. Hence, the free energy, at any point $\mathbf{X}$, is based on kinematic decomposition (3) and expressed by the unique *decoupled* representation

$$\Psi = U(\mathbf{X}; J) + \overline{\Psi}(\mathbf{X}; \overline{\mathbf{C}}, \mathbf{A}, \mathbf{B}) + \sum_{\alpha=1}^{m} \overline{\Upsilon}_\alpha(\mathbf{X}; \overline{\mathbf{C}}, \mathbf{A}, \mathbf{B}, \overline{\mathbf{\Gamma}}_\alpha)\,, \tag{6}$$

valid over some closed time interval $t \in [0, T]$. The first two terms on the right hand side of eq. (6) characterize the *equilibrium state* of the viscoelastic solid at fixed $\mathbf{F}$ as $t \to \infty$, which is a state of balance, while the third term, the free energy $\sum_{\alpha=1}^{m} \overline{\Upsilon}_\alpha$, characterizes the *non-equilibrium state*, i.e. the relaxation and creep behavior. The given strictly convex function U is responsible for the volumetric *elastic* response of the material, which only depends on the position $\mathbf{X}$ and on J. The given convex function $\overline{\Psi}$ is responsible for the isochoric *elastic* response. The representation (6) is well-suited for numerical implementation (see, for example, SIMO *et al.* [1985], SIMO & TAYLOR [1991] and HOLZAPFEL & GASSER [2001] amongst others).

Now we particularize the second law of thermodynamics through the Clausius-Planck inequality, i.e. $\mathcal{D}_{\text{int}} = \mathbf{S} : \dot{\mathbf{C}}/2 - \dot{\Psi} \geq 0$, where $\mathcal{D}_{\text{int}}$ is the internal dissipation (local entropy production). By computing the rate of change of Ψ and using the chain rule, we find that

$$\left(\mathbf{S} - J\frac{\mathrm{d}U}{\mathrm{d}J}\mathbf{C}^{-1} - 2\frac{\partial \overline{\Psi}}{\partial \mathbf{C}} - \sum_{\alpha=1}^{m} 2\frac{\partial \overline{\Upsilon}_\alpha}{\partial \mathbf{C}} \right) : \frac{1}{2}\dot{\mathbf{C}} - \sum_{\alpha=1}^{m} \frac{\partial \overline{\Upsilon}}{\partial \overline{\mathbf{\Gamma}}_\alpha} : \dot{\overline{\mathbf{\Gamma}}}_\alpha \geq 0\,. \tag{7}$$

In deriving (7) we used the properties $\dot{J} = \partial J/\partial \mathbf{C} : \dot{\mathbf{C}} = J\mathbf{C}^{-1} : \dot{\mathbf{C}}/2$ and $\dot{\overline{\mathbf{C}}} = 2(\partial \overline{\mathbf{C}}/\partial \mathbf{C}) : \dot{\mathbf{C}}/2$.

In order to satisfy $\mathcal{D}_{\text{int}} \geq 0$ for all admissible processes we apply the standard Coleman-Noll procedure (see COLEMAN & NOLL [1963] and COLEMAN & GURTIN [1967]). For arbitrary choices of $\dot{\mathbf{C}}$, we deduce the constitutive equations for compressible hyperelasticity and a remainder inequality governing the non-negativeness of the internal dissipation. In particular, the stress response constitutes an additive split of the second Piola-Kirchhoff stress tensor into purely *volumetric* and *isochoric* contributions, i.e. $\mathbf{S}_{\text{vol}}$ and $\mathbf{S}_{\text{iso}}$, $\mathbf{Q}_\alpha$, $\alpha = 1, \ldots, m$, respectively. We write

$$\mathbf{S} = 2\,\frac{\partial \Psi}{\partial \mathbf{C}} = \mathbf{S}_{\text{vol}} + \mathbf{S}_{\text{iso}} + \sum_{\alpha=1}^{m} \mathbf{Q}_\alpha\,. \tag{8}$$

This split is based on the definitions

$$\mathbf{S}_{\text{vol}} = J\frac{\mathrm{d}U(\mathbf{X}; J)}{\mathrm{d}J}\mathbf{C}^{-1}\,, \qquad \mathbf{S}_{\text{iso}} = 2\frac{\partial \overline{\Psi}(\mathbf{X}; \overline{\mathbf{C}}, \mathbf{A}, \mathbf{B})}{\partial \mathbf{C}}\,, \qquad \mathbf{Q}_\alpha = 2\frac{\partial \overline{\Upsilon}_\alpha(\mathbf{X}; \overline{\mathbf{C}}, \mathbf{A}, \mathbf{B}, \overline{\mathbf{\Gamma}}_\alpha)}{\partial \mathbf{C}} \tag{9}$$

of the volumetric *elastic* stress contribution $\mathbf{S}_{\text{vol}}$, the isochoric *elastic* stress contribution $\mathbf{S}_{\text{iso}}$ and the isochoric *viscoelastic* stress contributions $\mathbf{Q}_\alpha$, $\alpha = 1, \ldots, m$. The stresses $\mathbf{Q}_\alpha$ may be interpreted as *non-equilibrium stresses* in the sense of non-equilibrium thermodynamics, so that the free energy $\overline{\Upsilon}_\alpha$ takes on the form

$$\overline{\Upsilon}_\alpha = \int_{\mathbf{C}} \mathbf{Q}_\alpha(\mathbf{X}; \overline{\mathbf{C}}^*, \mathbf{A}, \mathbf{B}, \overline{\mathbf{\Gamma}}_\alpha) : \frac{1}{2}\mathrm{d}\mathbf{C}^*\,, \qquad \alpha = 1, \ldots, m\,, \tag{10}$$

(for a detailed exposition of the thermodynamic background see the text by HOLZAPFEL [2000], which contains further references). Since we agreed that the time-dependent response of the volumetric contribution is neglected, the tensor quantities $\mathbf{Q}_\alpha$ describe purely isochoric stresses, so that $\mathbf{Q}_\alpha : \mathbf{C} = 0$, $\alpha = 1, \dots, m$. The internal dissipation is given by

$$\mathcal{D}_{\rm int} = \sum_{\alpha=1}^{m} \mathbf{Q}_\alpha : \dot{\overline{\mathbf{\Gamma}}}_\alpha \geq 0 \,, \tag{11}$$

with the internal constitutive equations $\mathbf{Q}_\alpha = -\partial \overline{\Upsilon}_\alpha / \partial \overline{\mathbf{\Gamma}}_\alpha$. Through analogy with the equilibrium equations for the linear viscoelastic solid $\mathbf{Q}_\alpha$ is interpreted as the non-equilibrium stress in the system as introduced above. The internal constitutive equations restrict the free energy $\sum_{\alpha=1}^{m} \Upsilon_\alpha$ in view of $(9)_3$. Note that for arbitrary elastic processes $\dot{\overline{\mathbf{\Gamma}}}_\alpha = \mathbf{O}$, and hence the internal dissipation $\mathcal{D}_{\rm int}$ is zero (the material is considered to be elastic).

This constitutive framework is now used for the development of the internal variable model to describe the material behavior of arterial layers.

3.2 Energy function for the elastic response of arterial layers

To study the elastic response of healthy young arterial segments we model the arterial wall as a two-layer tube (media and adventitia). Each layer of the arterial wall is considered as a thick-walled composite structure reinforced by two families of *collagen fibers* which are continuously embedded in a *non-collageneous matrix material*. The fibers are helically wound along the arterial axis and symmetrically disposed with respect to the axis. Note, however, that the orientations of the fibers in the two layers are different. We postulate the change of the free energy within an elastic process at any point $\mathbf{X} \in (\Omega_0 \cup \partial\Omega_0)_{\rm M}$ in the media $\rm M$ and at any point $\mathbf{X} \in (\Omega_0 \cup \partial\Omega_0)_{\rm A}$ in the adventitia $\rm A$ according to the decoupled form

$$\left.\begin{aligned} \Psi_{\rm M} &= U_{\rm M}(\mathbf{X}; J) + \overline{\Psi}_{\rm M}(\mathbf{X}; \overline{\mathbf{C}}, \mathbf{A}_{\rm M}, \mathbf{B}_{\rm M}), \\ \Psi_{\rm A} &= U_{\rm A}(\mathbf{X}; J) + \overline{\Psi}_{\rm A}(\mathbf{X}; \overline{\mathbf{C}}, \mathbf{A}_{\rm A}, \mathbf{B}_{\rm A}), \end{aligned}\right\} \tag{12}$$

valid in time interval $t \in [0, T]$.

The terms $U_{\rm M}$ and $U_{\rm A}$, associated with the respective media $\rm M$ and adventitia $\rm A$, denote Lagrange-multiplier terms which vanish for the incompressible limit. The functions $\overline{\Psi}_{\rm M}$ and $\overline{\Psi}_{\rm A}$ are associated with the isochoric elastic responses of the media and adventitia, respectively. They depend on the respective points, the modified strain $\overline{\mathbf{C}}$ and on the (second-order) tensors $\mathbf{A}_j$ and $\mathbf{B}_j$, $j = {\rm M}, {\rm A}$, which characterize the structure of the media and adventitia, i.e. the orientation of the collagen fibers. The structural tensors are defined by the tensor products

$$\mathbf{A}_j = \mathbf{a}_{0\,j} \otimes \mathbf{a}_{0\,j}, \qquad \mathbf{B}_j = \mathbf{b}_{0\,j} \otimes \mathbf{b}_{0\,j}, \qquad j = {\rm M}, {\rm A}, \tag{13}$$

with the two unit vector fields $\mathbf{a}_0 : \Omega_0 \to \mathbb{R}^3$ and $\mathbf{b}_0 : \Omega_0 \to \mathbb{R}^3$, describing the basic geometry of the two families of fibers in the reference configuration. They characterize the two preferred fiber directions in each point $\mathbf{X} \in \Omega_0$ which are determined from the automatic technique

discussed in Section 2.2. In a cylindrical polar coordinate system, the components of $\mathbf{a}_{0\,j}$ and $\mathbf{b}_{0\,j}$ have the forms

$$[\mathbf{a}_{0\,j}] = \begin{bmatrix} 0 \\ \cos\varphi_j \\ \sin\varphi_j \end{bmatrix}, \qquad [\mathbf{b}_{0\,j}] = \begin{bmatrix} 0 \\ \cos\varphi_j \\ -\sin\varphi_j \end{bmatrix}, \quad j = \mathrm{M}, \mathrm{A}, \tag{14}$$

where φ_{M} and φ_{A} are the (mean) angles between the collagen fibers (arranged in symmetrical spirals) and the circumferential direction in the media and adventitia.

The next goal is to particularize the isochoric contributions $\overline{\Psi}_j$, $j = \mathrm{M}, \mathrm{A}$. According to SPENCER [1984], the integrity basis for the three symmetric second-order tensors $\overline{\mathbf{C}}$, $\mathbf{A}$, $\mathbf{B}$ consists of nine invariants and we may alternatively express the functions $\overline{\Psi}_j$ in terms of these nine invariants. However, in order to minimize the number of material parameters (which are associated with the collagen and the non-collagenous matrix material varying along the arterial tree, with aging, hypertension etc.) we consider expressions in terms of three invariants only. Clearly, here we are dealing with two different materials, however, the mechanical characteristics of the media and adventitia are similar, so that we use the *same* form of free-energy function (but a *different* set of material parameters) for each layer. Thus, we propose the particularizations of $\overline{\Psi}_j$ as

$$\left.\begin{aligned} \overline{\Psi}_{\mathrm{M}} &= \frac{c_{\mathrm{M}}}{2}(\bar{I}_1 - 3) + \frac{k_{1\,\mathrm{M}}}{2k_{2\,\mathrm{M}}} \sum_{i=4,6} \left\{ \exp[k_{2\,\mathrm{M}}(\bar{I}_{i\,\mathrm{M}} - 1)^2] - 1 \right\}, \\ \overline{\Psi}_{\mathrm{A}} &= \frac{c_{\mathrm{A}}}{2}(\bar{I}_1 - 3) + \frac{k_{1\,\mathrm{A}}}{2k_{2\,\mathrm{A}}} \sum_{i=4,6} \left\{ \exp[k_{2\,\mathrm{A}}(\bar{I}_{i\,\mathrm{A}} - 1)^2] - 1 \right\}, \end{aligned}\right\} \tag{15}$$

with the (positive) material parameters c_{M}, $k_{1\,\mathrm{M}}$, $k_{2\,\mathrm{M}}$ and c_{A}, $k_{1\,\mathrm{A}}$, $k_{2\,\mathrm{A}}$ associated with the media M and adventitia A, respectively. The parameters c and k_1 are stress-like material parameters, while k_2 is a dimensionless parameter. The first modified invariant is characterized by

$$\bar{I}_1(\overline{\mathbf{C}}) = \mathbf{I} : \overline{\mathbf{C}}, \tag{16}$$

and

$$\bar{I}_{4\,j} = \begin{cases} \mathbf{A}_j : \overline{\mathbf{C}}, & \text{for} \quad \mathbf{A}_j : \overline{\mathbf{C}} \geq 1, \\ 1, & \text{for} \quad \mathbf{A}_j : \overline{\mathbf{C}} < 1, \end{cases} \qquad \bar{I}_{6\,j} = \begin{cases} \mathbf{B}_j : \overline{\mathbf{C}}, & \text{for} \quad \mathbf{B}_j : \overline{\mathbf{C}} \geq 1, \\ 1, & \text{for} \quad \mathbf{B}_j : \overline{\mathbf{C}} < 1, \end{cases} \tag{17}$$

are two additional invariants associated with each layer $j = \mathrm{M}, \mathrm{A}$ (the restrictions imposed on these invariants ensure that the collagen fibers cannot be subject to compressive strains). The invariants $\bar{I}_4$ and $\bar{I}_6$ have a clear physical interpretation. They are the squares of the stretches in the two families of (collagen) fibers and represent stretch measures.

ROACH & BURTON [1957] identified the mechanical contributions of elastin and collagen in the human iliac artery. They concluded that elastin, as a main contributor to the normal pulsatile behavior of arteries, bears loads primarily at low stresses and strains, while at high strains the collagen fibers dominate the mechanical behavior of the artery. The mechanical response of

the non-collagenous matrix material, composed mainly of elastin fibers, is similar to that of a rubber-like material, and is hence assumed to be isotropic and modeled as a (classical) neo-Hookean material, which is expressed in terms of the first modified invariant $\bar{I}_1$ (the first parts of the isochoric strain-energy functions $\overline{\Psi}$ in eqs. (15)). The wavy collagen fibers are relaxed at low strains (pressures), but are progressively 'recruited' at increasing strains and dominate the mechanical behavior of the artery at high strains. The 'recruitment' of the collagen fibers leads to the stiffening effect and the characteristic strongly anisotropic mechanical behavior of arteries. This is modeled by an exponential function and expressed in terms of the invariants $\bar{I}_4$ and $\bar{I}_6$ (the second parts of the functions $\overline{\Psi}$ in eqs. (15)).

In contrast to many other (classical) models based on phenomenological approaches the proposed three-dimensional structural model has the main advantage that the material parameters have immediate physical meaning. The model is consistent with both mechanical and mathematical requirements and is able to capture the main characteristics of the arterial response in an accurate manner, as pointed out by HOLZAPFEL *et al.* [2000], in which a detailed comparison with other prominent (elastic) material models is also given. In addition, note that all mathematical expressions of the constitutive model problem presented above are limited to stresses and strains in the *physiological* range. They do not apply when the artery is stressed far beyond the physiological range where permanent deformations occur and plastic constitutive models of arterial walls are required. For an extension of the presented model to the elastoplastic domain the reader is referred to the more general framework of GASSER & HOLZAPFEL [2001], which also focus on the implementation in a finite element program.

3.3 Decoupled volumetric-isochoric stress response

For each arterial layer the stress response is derived from the associated Helmholtz free-energy function. According to the constitutive framework discussed in Section 3.1.2 we arrive at the (second Piola-Kirchhoff) stress response

$$\left.\begin{aligned} \mathbf{S}_{\mathrm{M}} &= (Jp\mathbf{C}^{-1})_{\mathrm{M}} + \sum_{a=1,4,6} (\mathbf{S}_{\mathrm{iso}\,a} + \sum_{\alpha=1}^{m} \mathbf{Q}_{\alpha\,a})_{\mathrm{M}}, \\ \mathbf{S}_{\mathrm{A}} &= (Jp\mathbf{C}^{-1})_{\mathrm{A}} + \sum_{a=1,4,6} (\mathbf{S}_{\mathrm{iso}\,a} + \sum_{\alpha=1}^{m} \mathbf{Q}_{\alpha\,a})_{\mathrm{A}} \end{aligned}\right\} \tag{18}$$

for the media and adventitia, respectively (compare with the mathematical structure $(8)_2$). However, $\mathbf{S}_{\mathrm{iso}}$, $\mathbf{Q}_\alpha$ are replaced by $\mathbf{S}_{\mathrm{iso}\,a}$, $\mathbf{Q}_{\alpha\,a}$ signifying the a-th constituent of the arterial layer ($a = 1$ is associated with the non-collagenous matrix material and $a = 4, 6$ with the two families of collagen fibers). We recall that the index α stands for the number of viscoelastic processes. Note that for the case $a = 1$ isotropy is recovered as a special case.

Considering the particularization (15) of the free energy and the decoupled representation of the kinematics according to Section 3.1.1, we may express the isochoric elastic stress contributions (eq. $(9)_2$) in the alternative form

$$\mathbf{S}_{\mathrm{iso}\,a} = J^{-2/3}\mathbb{P} : (2\psi_a \mathbf{D}_a), \qquad (a = 1, 4, 6; \text{ no summation}), \tag{19}$$

which is used in relations (18). We introduced the useful definitions

$$p = \frac{\mathrm{d}U(J)}{\mathrm{d}J}\,, \qquad \psi_a = \frac{\partial\overline{\Psi}(\bar{I}_1, \bar{I}_4, \bar{I}_6)}{\partial\bar{I}_a}\,, \qquad a = 1, 4, 6 \tag{20}$$

of the stress functions (suppressing the dependency on the reference point $\mathbf{X}$ in the arguments of the energies U and $\overline{\Psi}$), i.e. the hydrostatic pressure p and ψ_a, $a = 1, 4, 6$, which are affected by the special choice of U and $\overline{\Psi}$ (the material). In addition, in eq. (19) we have introduced the definitions

$$\mathbb{P} = \mathbb{I} - \frac{1}{3}\mathbf{C}^{-1} \otimes \mathbf{C}\,, \qquad \mathbf{D}_a = \frac{\partial\bar{I}_a}{\partial\overline{\mathbf{C}}}\,, \qquad a = 1, 4, 6 \tag{21}$$

of kinematic quantities, i.e. the (fourth-order) projection tensor $\mathbb{P}$ and the second-order tensors $\mathbf{D}_a$, $a = 1, 4, 6$. Note that $\mathbb{P}$ furnishes the physically correct deviator in the material description (see HOLZAPFEL [2000]). From eq. $(21)_2$ we may conclude, using definitions (16), (17), that $\mathbf{D}_1 = \mathbf{I}$, $\mathbf{D}_4 = \mathbf{A}$ and $\mathbf{D}_6 = \mathbf{B}$. With the given functions (15), it is also straightforward to particularize eq. $(20)_2$ in order to obtain

$$\psi_1 = c/2\,, \tag{22}$$

$$\psi_4 = k_1(\bar{I}_4 - 1)\exp\left[k_2(\bar{I}_4 - 1)^2\right]\,, \tag{23}$$

$$\psi_6 = k_1(\bar{I}_6 - 1)\exp\left[k_2(\bar{I}_6 - 1)^2\right]\,. \tag{24}$$

As seen from definition (19) (with eqs. (22)–(24)) the stress response consists of purely *isotropic* contributions $\mathbf{S}_{\mathrm{iso}\,1}$ due to the matrix material, and *anisotropic* contributions $\mathbf{S}_{\mathrm{iso}\,4}$, $\mathbf{S}_{\mathrm{iso}\,6}$ due to the two families of fibers, which characterize decoupled stresses (associated only with the fibers).

The non-equilibrium states of the arterial layers are associated with the additional tensor variables $\mathbf{Q}_{\alpha\,a}$ for $\alpha = 1, \ldots, m$ and $a = 1, 4, 6$. They are zero at a state of thermodynamic equilibrium, which implies that the anisotropic material responds perfectly elastically. The non-equilibrium stresses are governed by complementary equations of evolution, as discussed in the following section.

3.3.1 Evolution equations for the non-equilibrium stresses

In order to determine how a viscoelastic process in an artery evolves, we have to postulate additional equations governing the non-equilibrium stresses.

Hysteresis loops of arterial tissues are known to be not very sensitive to strain rates over several decades (see, for example, the study by TANAKA & FUNG [1974] performed for various arteries of dogs). This is also true for other types of biological soft tissues such as articular cartilage (WOO *et al.* [1979]) or the mesentery (CHEN & FUNG [1973]). Hence, we have to select a rheological model which considers this characteristic feature. Classical mechanical devices such as the *Maxwell model* (spring in series with a dashpot), the *Kelvin-Voigt model*

(spring in parallel with a dashpot) or a device of the *'standard solid'* type, which is a free spring on one end and one Maxwell element arranged in parallel, are not able to represent the typical viscoelastic behavior of soft tissues. The damping mechanisms of these devices are strongly frequency dependent and are not suitable candidates for formulating meaningful evolution equations. However, a mechanical device which is composed of a number of springs and dashpots gives the required viscoelastic behavior (see, for example, FUNG [1993], Section 7.6, for more details and references).

For this reason we extend the attractive one-dimensional *generalized Maxwell model* to the three-dimensional region. The generalized Maxwell model may be seen as a mechanical device with a *free spring* on one end and an arbitrary number m of *Maxwell elements* arranged in parallel (see, for example, HOLZAPFEL [2000], Section 6.10). The more Maxwell elements and associated (different) relaxation times used the nearer is the response to constant damping over a wide frequency spectrum.

Hence, for each of the (isochoric) non-equilibrium stresses, *separately* for each α and constituent a of the arterial layer, we formulate an evolution equation. We assume the set of linear differential equations

$$\dot{\mathbf{Q}}_{\alpha\,a} + \frac{\mathbf{Q}_{\alpha\,a}}{\tau_{\alpha\,a}} = \beta^{\infty}_{\alpha\,a}\dot{\mathbf{S}}_{\mathrm{iso}\,a}\,, \qquad \mathbf{Q}_{\alpha\,a}|_{t=0} = \mathbf{O}\,, \qquad (a = 1,4,6\text{; no summation}), \text{ and } \alpha = 1,\dots,m) \tag{25}$$

valid for some semi-open time interval $t \in (0,T]$ and for small perturbations away from the equilibrium state. The initial conditions $(25)_2$ ensure that the reference configuration has no viscoelastic stress contribution. The constants $\beta^{\infty}_{\alpha\,a} \in [0,\infty)$ introduced are given so-called *free-energy factors*, which are non-dimensional and associated with the relaxation times $\tau_{\alpha\,a} \in (0,\infty)$, which describe the rate of decay of the stress and strain in a viscoelastic process.

Closed-form solutions of the linear equations $(25)_1$ may be represented by the simple convolution integrals

$$\mathbf{Q}_{\alpha\,a} = \int_{t=0^+}^{t=T} \exp[-(T-t)/\tau_{\alpha\,a}]\beta^{\infty}_{\alpha\,a}\dot{\mathbf{S}}_{\mathrm{iso}\,a}(t)\mathrm{d}t \quad , \tag{26}$$

for $a = 1,4,6$ and $\alpha = 1,\dots,m$. The typical features of anisotropic arterial response in the large strain domain is now described completely by the constitutive equations (18), with expressions (19)–(24) and (26).

4 Finite element formulation

In order to capture the complex deformation behavior of arteries, which are considered here as incompressible materials, we employ the well established finite element methodology. In particular, we are interested in a suitable variational approach capable of representing the purely isochoric response in an efficient way.

4.1 Three-field variational principle

The equivalent counterpart of the strong form of the initial boundary-value problem, as expressed by the set (4), (5), is its *weak form* (see HOLZAPFEL [2000], Section 8.2). The weak form leads to the fundamental principle of virtual work to be solved for the *single* unknown displacement field **u**. However, it is known that such a single-field variational principle is not appropriate for solving problems involving constrained materials, which we want to study here. The analysis of, for example, nearly incompressible or incompressible constitutive responses is associated with numerical difficulties (*'locking'* and *'checkerboard' phenomena*) and they perform rather poorly within the context of a (standard) Galerkin method. These difficulties, inherent in the conventional single-field variational approach, arise from the overstiffening of the system.

Here we outline briefly the mixed *Jacobian-pressure formulation* emanating from a three-field Hu-Washizu variational approach proposed by SIMO *et al.* [1985] (for applications in hyperelasticity see, for example, SIMO [1987], SIMO & TAYLOR [1991], WEISS *et al.* [1996], HOLZAPFEL & GASSER [2001]; for applications in large-strain plasticity the reader is referred to the works by SIMO *et al.* [1985], SIMO & MIEHE [1992], MIEHE [1996] among others). This type of mixed formulation may be regarded as the nonlinear extension of the B-bar method, as proposed by HUGHES [2000], and overcomes these numerical difficulties. Thereby, the displacement field and two additional field variables are treated independently within finite element discretizations.

The functional, $\mathcal{L}$ say, is decomposed into three parts and takes advantage of the decoupled representation of the free energy according to (6). It is defined as

$$\mathcal{L}(\mathbf{u}, p, \tilde{J}; \lambda) = \Pi(\mathbf{u}, p, \tilde{J}) + \Pi_{\text{ext}}(\mathbf{u}) + \Pi_{\text{aug}}(\tilde{J}; \lambda)\,, \tag{27}$$

$$\Pi(\mathbf{u}, p, \tilde{J}) = \int_{\Omega_0} [U(\tilde{J}) + p(J(\mathbf{u}) - \tilde{J}) + \overline{\Psi}(\overline{\mathbf{C}}(\mathbf{u}), \mathbf{A}, \mathbf{B}) \tag{28}$$

$$+ \sum_{\alpha=1}^{m} \overline{\Upsilon}_\alpha(\overline{\mathbf{C}}(\mathbf{u}), \mathbf{A}, \mathbf{B}, \overline{\mathbf{\Gamma}}_\alpha(\mathbf{u}, t))]\mathrm{d}V\,, \tag{29}$$

$$\Pi_{\text{ext}}(\mathbf{u}) = -\int_{\Omega_0} \mathbf{B} \cdot \mathbf{u}\mathrm{d}V - \int_{\partial\Omega_{0\,\sigma}} \overline{\mathbf{T}} \cdot \mathbf{u}\mathrm{d}S\,, \tag{30}$$

$$\Pi_{\text{aug}}(\tilde{J}; \lambda) = \int_{\Omega_0} \lambda h(\tilde{J})\mathrm{d}V \tag{31}$$

(suppressing the dependency on **X** in the arguments of the functions), where Π_{ext} denotes the external potential energy. Here, **u** is the common displacement field, while $p \in L^2(\Omega_0)$ and $\tilde{J} \in L^2_+(\Omega_0)$ are additional *independent* field variables which may be identified as the hydrostatic pressure and the volumetric ratio (kinematic variable), respectively. The constraint condition $J = \tilde{J}$ is enforced by p.

Note, that the variational principle (27) is *augmented* by a continuously differentiable function

$h(\tilde{J}) : \mathbb{R}_+ \to \mathbb{R}$ that satisfies $h(1) = 0$ for $\tilde{J} = 1$, which is multiplied by a *Lagrange multiplier* $\lambda \in L^2(\Omega_0)$. For example,

$$h(\tilde{J}) = \tilde{J} - 1 \,, \qquad U(\tilde{J}) = \frac{\kappa}{2}(\tilde{J} - 1)^2 \tag{32}$$

are suitable candidates for the functions h and U, with $h(1) = 0$, $U(1) = 0$. Note that for the incompressible case the (positive) parameter $\kappa > 0$ serves as a user–specified *penalty* parameter which has no physical relevance.

Since the penalty parameter $\kappa > 0$ is assumed to be positive, $\mathrm{d}U^2(\tilde{J})/\mathrm{d}^2\tilde{J} > 0$ in $\mathbb{R}_+$, the function U, which may be viewed as a penalty function for $\tilde{J} = 1$, is convex. It is worthwhile mentioning that the augmented term prevents the (global) stiffness matrix from becoming increasingly ill-conditioned for increasing κ, a problem known from the penalty method. With the augmented term the incompressibility constraint, formulated in terms of the additional variable $\tilde{J}$, can be enforced up to an arbitrary precision.

We require that the solutions of the boundary-value problem, i.e. the *three* field variables $\mathbf{u}$, p and $\tilde{J}$, are stationary points of the functional $\mathcal{L}$. This leads to the set of *Euler-Langrange* equations in the weak forms

$$\left.\begin{aligned}
D_{\delta\mathbf{u}}\mathcal{L}(\mathbf{u},p,\tilde{J};\lambda) &= \int_{\Omega_0} \left(J(\mathbf{u})p\mathbf{C}^{-1}(\mathbf{u}) + 2\frac{\partial\overline{\Psi}(\overline{\mathbf{C}}(\mathbf{u}),\mathbf{A},\mathbf{B})}{\partial\mathbf{C}} \right. \\
&\quad \left. + \sum_{\alpha=1}^{m} 2\frac{\partial\overline{\Upsilon}_\alpha(\overline{\mathbf{C}}(\mathbf{u}),\mathbf{A},\mathbf{B},\overline{\mathbf{\Gamma}}_\alpha(\mathbf{u},t))}{\partial\mathbf{C}} \right) : \frac{1}{2}\delta\mathbf{C}(\mathbf{u})\mathrm{d}V + D_{\delta\mathbf{u}}\Pi_{\mathrm{ext}}(\mathbf{u}) = 0 \;, \\
D_{\delta p}\mathcal{L}(\mathbf{u},p,\tilde{J};\lambda) &= \int_{\Omega_0} (J(\mathbf{u}) - \tilde{J})\delta p\mathrm{d}V = 0 \;, \\
D_{\delta\tilde{J}}\mathcal{L}(\mathbf{u},p,\tilde{J};\lambda) &= \int_{\Omega_0} \left(\frac{\mathrm{d}U(\tilde{J})}{\mathrm{d}\tilde{J}} - p + \lambda\frac{\mathrm{d}h(\tilde{J})}{\mathrm{d}\tilde{J}} \right) \delta\tilde{J}\mathrm{d}V = 0 \;,
\end{aligned}\right\} \tag{33}$$

where $\delta(\bullet)$ denotes the first variation of the field variable $(\bullet)$. For the variational equation $(33)_1$, we require $\delta\mathbf{u}$ to be kinematically admissible, i.e. $\{\delta\mathbf{u} : \Omega_0 \to \mathbb{R}^3 | \delta\mathbf{u}|_{\partial\Omega_{0\,\mathrm{u}}} = \mathbf{0}\}$, and eqs. $(33)_2$ and $(33)_3$ hold for all δp and $\delta\tilde{J}$, respectively. The term $D_{\delta(\bullet)}\mathcal{L}$ denotes the directional derivative (Gâteaux derivative) of $\mathcal{L}$ at $\mathbf{x}$ in the direction of the field variable $(\bullet)$, and is defined through the expression

$$D_{\delta(\bullet)}\mathcal{L} = \left.\frac{\mathrm{d}}{\mathrm{d}\varepsilon}\right|_{\varepsilon=0} \mathcal{L}((\bullet) + \varepsilon\delta(\bullet)) \tag{34}$$

(see, for example, MARSDEN & HUGHES [1994]), where $D(\bullet)$ is the Gâteaux operator and ε is a scalar parameter.

If the local forms of eqs. $(33)_2$ and $(33)_3$ are satisfied, then p is identified as the hydrostatic pressure. Hence, according to definitions (9) and $(20)_1$ the first three terms on the right-hand side of the variational equation $(33)_1$ give precisely the second Piola-Kirchhoff stress tensor

S with the specification (18). Consequently, the integral in $(33)_1$ is the internal (mechanical) virtual work $\delta W_{\rm int}$, while the last term $D_{\delta\mathbf{u}}\Pi_{\rm ext}(\mathbf{u})$ in $(33)_1$, i.e. the directional derivative of $\Pi_{\rm ext}$ with respect to $\mathbf{u}$ in the arbitrary direction $\delta\mathbf{u}$, denotes the negative external (mechanical) virtual work $-\delta W_{\rm ext}$, and hence the variational equation $(33)_1$ characterizes precisely the virtual work equation in the material description and expresses equilibrium in the form $\delta W_{\rm int} = \delta W_{\rm ext}$.

4.2 Mixed finite element formulation and Uzawa update

In this section we outline briefly a finite element formulation that avoids numerical difficulties in the incompressible limit. The formulation is used for the solution of the momentum balance equation together with the augmented Lagrangian optimization technique and an Uzawa update algorithm (ARROW *et al.* [1958]), thereby avoiding ill-conditioning of the stiffness matrix associated with the penalty approach. The reason for the ill-conditioned stiffness matrix may be found in the significantly different magnitudes of the volumetric and isochoric components.

To construct efficient finite element approximations we use mixed interpolations for the Jacobian and the pressure. For the fields $\mathbf{X}$, $\mathbf{u}$ and $\delta\mathbf{u}$ we use isoparametric interpolations and obtain

$$\mathbf{X}_{\rm h} = \sum_{k=1}^{n_{\rm node}} N_k(\boldsymbol{\xi})\mathbf{X}_k\,, \qquad \mathbf{u}_{\rm h} = \sum_{k=1}^{n_{\rm node}} N_k(\boldsymbol{\xi})\mathbf{u}_k\,, \qquad \delta\mathbf{u}_{\rm h} = \sum_{k=1}^{n_{\rm node}} N_k(\boldsymbol{\xi})\delta\mathbf{u}_k\,, \tag{35}$$

where the subscript $(\bullet)_{\rm h}$ indicates the discrete (finite-dimensional) counterpart to quantity $(\bullet)$. The reference position, and the real and virtual displacements of the element node k are denoted by $\mathbf{X}_k$, and $\mathbf{u}_k$ and $\delta\mathbf{u}_k$, respectively. The subscript $(\bullet)_k$ is an index running between 1 and the total number of element nodes, denoted by $n_{\rm node}$. In eqs. (35), $\boldsymbol{\xi} = \{\xi_1, \xi_2, \xi_3\} \in \Omega_\square$ are the local element coordinates (the natural coordinates), where $\Omega_\square = \{\boldsymbol{\xi} \in \mathbb{R}^3 | (-1,1) \times (-1,1) \times (-1,1)\}$ characterize the domain of the *parent element*, i.e. a biunit cube. The isoparametric interpolation function associated with node k, is denoted by $N_k(\boldsymbol{\xi})$ and defined in $\Omega_\square$ (for a more detailed explanation of these standard concepts, see, for example, HUGHES [2000]). Now we shall assume that the interpolation functions are *tri-linear* and expressed in the form $N_k(\boldsymbol{\xi}) = \frac{1}{8}(1+\xi_{1k}\xi_1)(1+\xi_{2k}\xi_2)(1+\xi_{3k}\xi_3)$, $k = 1, \ldots, n_{\rm node} = 8$.

With eqs. (35) it is straightforward to compute the discrete current position $\mathbf{x}_{\rm h} = \mathbf{X}_{\rm h} + \mathbf{u}_{\rm h}$ and the discrete deformation gradient $\mathbf{F}_{\rm h} = \sum_{k=1}^{n_{\rm node}} \mathbf{x}_k \otimes \boldsymbol{\nabla}_{\mathbf{X}} N_k(\boldsymbol{\xi})$, where the standard expressions

$$\boldsymbol{\nabla}_{\mathbf{X}} N_k(\boldsymbol{\xi}) = \frac{\partial N_k(\boldsymbol{\xi})}{\partial \mathbf{X}_{\rm h}} = \mathbf{J}_{\rm h}^{-\rm T} \frac{\partial N_k}{\partial \boldsymbol{\xi}}, \qquad \mathbf{J}_{\rm h} = \frac{\partial \mathbf{X}_{\rm h}}{\partial \boldsymbol{\xi}} = \sum_{k=1}^{n_{\rm node}} \mathbf{X}_k \otimes \boldsymbol{\nabla}_{\boldsymbol{\xi}} N_k \tag{36}$$

are to be used. Therein, $\boldsymbol{\nabla}_{(\bullet)} N_k$ denotes the gradient of the scalar function N_k with respect to the coordinates $(\bullet)$ and $\mathbf{J}_{\rm h}$ is the *Jacobian operator*, which transforms the gradient $\boldsymbol{\nabla}_{\boldsymbol{\xi}} N_k$ to the gradient $\boldsymbol{\nabla}_{\mathbf{X}} N_k$. With the fundamental kinematic expression $\mathbf{F}_{\rm h}$ we are able to compute any strain and associated stress quantity.

In addition, for the independent (dilatation and pressure) variables $\tilde{J}$ and p, we introduce the same *constant* (discontinuous) interpolation functions over a given element domain without

having to satisfy continuity across the element boundaries (SIMO *et al.* [1985]). Thus, we write $\tilde{J}_{\rm h} = \bar{\tilde{J}}$ and $p_{\rm h} = \bar{p}$, where the symbol $(\bar{\bullet})$ denotes the constant interpolation function. Since the additional (independent) variables $\bar{\tilde{J}}$ and $\bar{p}$ can be eliminated at the element level (static condensation) we get

$$\bar{\tilde{J}} = \frac{v_{\rm e}}{V_{\rm e}}\,, \qquad \bar{p} = \left(\lambda_{\rm h}\frac{{\rm d}h(\bar{\tilde{J}})}{{\rm d}\bar{\tilde{J}}} + \frac{{\rm d}U(\bar{\tilde{J}})}{{\rm d}\bar{\tilde{J}}}\right)\Bigg|_{\bar{\tilde{J}}=v_{\rm e}/V_{\rm e}}\,, \tag{37}$$

where $v_{\rm e}$ and $V_{\rm e}$ are element volumes in the current and reference configurations, respectively. Recalling eqs. (32), the mean pressure $(37)_2$ yields $\bar{p} = \lambda_{\rm h} + \kappa(v_{\rm e} - V_{\rm e})/V_{\rm e}$, and for $\bar{\tilde{J}} \to 1$ we obtain the limit $\bar{p} \to \lambda_{\rm h}$. Hence, the expression $(37)_2$ for the constant pressure $\bar{p}$ (with $\bar{\tilde{J}}$ determined in $(37)_1$) is therefore used in the discrete form of the internal virtual work. This type of formulation is known as the mean dilatation technique, leading to the $Q1/P0$-element, a procedure which goes back to NAGTEGAAL *et al.* [1974]. This approach may be regarded as the nonlinear extension of the B-bar method, as proposed by HUGHES [2000].

The nonlinear (initial boundary-value) problem is solved by means of an incremental/iterative solution technique of Newton's type until convergence is achieved. Consequently, a sequence of linearized problems leads to solution increments at fixed λ. To enforce the incompressibility constraint a nested iteration of *Uzawa's* type is performed on the finite element level at fixed **u**, p, $\tilde{J}$ until the magnitude of $h = (\tilde{J} - 1)$ is less than a given tolerance of accuracy. According to SIMO & TAYLOR [1991], the Lagrange multiplier λ may then be determined by the standard update procedure $\lambda \Leftarrow \lambda + \kappa h$ of a typical $Q1/P0$ mixed finite element.

5 Representative numerical examples

Two numerical examples are now chosen to investigate the characteristic viscoelastic (relaxation and creep) behavior of a healthy and young arterial segment under various (static and dynamic) boundary loadings. They are supposed to show the physical mechanisms of the model outlined in Section 3, and to document finite element results which are in good qualitative agreement with experimental data.

Since we consider an arterial segment with no pathological changes of the innermost layer, the intimal components have negligible (solid) mechanical contributions, we approximate the arterial segment by two separate thick-walled fiber-reinforced circular layers, i.e. the media and the adventitia, which behave incompressibly.

In order to consider residual stresses (and strains) associated with the unloaded configuration, we introduce opened-up (reference) configurations for the media and adventitia. Each arterial layer in the reference configuration is assumed to be unstressed (the residual stresses are entirely removed by leaving all other properties of the material unchanged) and taken to correspond to an open sector of a circular cylindrical tube with opening angle α, wall thickness H, inner radius $R_{\rm i}$ and length L, as indicated in Figure 3. We assume that the media occupies $2/3$ of the arterial wall thickness. The collagen fibers are symmetrically disposed with respect to the axis and the

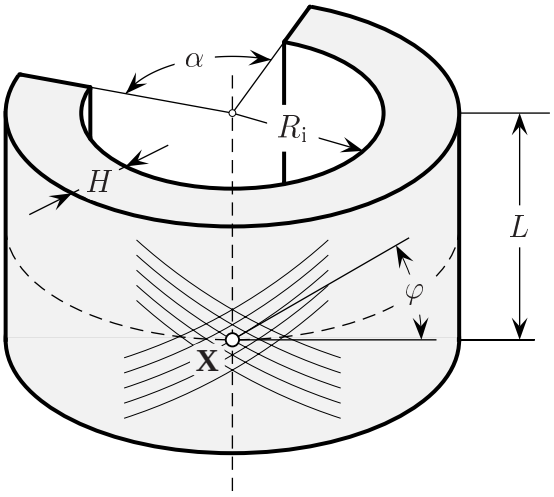

Media	$R_{i\,M} = 3.302\,(\mathrm{mm})$ $H_M = 0.493\,(\mathrm{mm})$ $\varphi_M = 10.0°$ $\alpha_M = 160.0°$
Adventitia	$R_{i\,A} = 3.482\,(\mathrm{mm})$ $H_A = 0.247\,(\mathrm{mm})$ $\varphi_A = 40.0°$ $\alpha_A = 120.0°$

$L = 45.0\,(\mathrm{mm})$

Figure 3: Opened-up (stress-free) configuration of an arterial layer and associated geometrical data for the media and adventitia.

orientations of the fibers, characterized by the angle φ at a reference point **X**, are different in the two layers. Specific geometrical data for each layer are summarized in Figure 3.

The unloaded but stressed circular cylindrical shape of the arterial segment, for which $\alpha = 0.0°$, is generated by application of an initial (pure) bending deformation (for more details see HOLZAPFEL *et al.* [2000]). By assuming no changes in thickness during this deformation, the dimensions of the arterial cross-section coincide then with those of a human left anterior descending coronary artery (LAD), as documented in CARMINES *et al.* [1991]. However, therein no geometrical information about separated opened-up configurations of arterial layers is reported. Note that, in general, there may also be residual stresses in the axial direction of the arterial segment (VOSSOUGHI [1992]), but we neglect this in the present study.

The proposed energy function has been implemented in Version 7.3 of the multi-purpose finite element analysis program FEAP, originally developed by *R.L. Taylor* and documented in TAYLOR [2000]. The three-dimensional finite element analysis is based on 8-node brick elements. During the computation the top and bottom faces of the tube are assumed to remain planar. Since the expected stress and strain states are homogeneous in the circumferential direction, only a sector of the structure (a wedge of any angle) is discretized by eight finite elements (five for the media and three for the adventitia) and analyzed. Each node at the media/adventitia interface is linked together and common symmetrical boundary conditions for the structure are applied.

5.1 Identification of the material parameters

In order to obtain meaningful results we need a complete set of elastic *and* viscoelastic material parameters based on experimental data. Since these parameters are not known *a priori*, we propose an identification process for quantifying the required material parameters involved

in the constitutive model outlined in Section 3. The decomposition of the model into elastic and viscoelastic responses allows separate determination of the material parameters associated with the elastic and viscoelastic parts. In this section the identification process for the material parameters is described in detail.

5.1.1 Elastic material parameters

The (elastic) material parameters c_i, $k_{1\,i}$, $k_{2\,i}$, $i = \mathrm{M}, \mathrm{A}$, which are involved in the strain-energy functions (15), were fitted to the experimental data of a human left anterior descending coronary artery (LAD), as given in CARMINES *et al.* [1991]. For purposes which were made clear by HOLZAPFEL *et al.* [2000] we set $c_{\mathrm{M}} = 10 c_{\mathrm{A}}$. The penalty parameters κ_i, $i = \mathrm{M}, \mathrm{A}$, see eq. $(32)_2$, were chosen to be $10^4\,(\mathrm{kPa})$. The resulting values are summarized in Table 1.

Media	**Adventitia**
$c_{\mathrm{M}} = 27.0\,(\mathrm{kPa})$	$c_{\mathrm{A}} = 2.7\,(\mathrm{kPa})$
$k_{1\,\mathrm{M}} = 0.64\,(\mathrm{kPa})$	$k_{1\,\mathrm{A}} = 5.1\,(\mathrm{kPa})$
$k_{2\,\mathrm{M}} = 3.54\,(-)$	$k_{2\,\mathrm{A}} = 15.4\,(-)$
$\kappa_{\mathrm{M}} = 10^4\,(\mathrm{kPa})$	$\kappa_{\mathrm{A}} = 10^4\,(\mathrm{kPa})$

Table 1: Elastic material parameters c_i, $k_{1\,i}$, $k_{2\,i}$, $i = \mathrm{M}, \mathrm{A}$, for the media M and adventitia A, and penalty parameters κ_i.

5.1.2 Viscoelastic material parameters

As mentioned above, the dissipation of arterial soft tissues in cyclic loading is relatively insensitive over a wide frequency spectrum. The intention now is to use experimental data for a *human* LAD, since it has already been used for the identification of the elastic material parameters. Unfortunately, only a few experimental studies in the literature deal with the *viscoelastic* behavior of human LADs in a multi-dimensional regime (for *in vitro* inflation tests see, for example, the data book edited by ABÈ *et al.* [1996]).

For the present work, we adopt the *in vitro* study by GOW & HADFIELD [1979], in which dynamic ($\mathsf{C}_{\mathrm{dyn}}$) and static ($\mathsf{C}_{\mathrm{stat}}$) incremental (Young's) moduli for three human coronary arteries were measured at an internal pressure of $p_{\mathrm{i}} = 13.33\,(\mathrm{kPa})$, i.e. 100 mm Hg. The mean ratio of $\mathsf{C}_{\mathrm{dyn}}/\mathsf{C}_{\mathrm{stat}}$ was obtained as 2.33. This value is based on measurements at 2 Hz. Unfortunately, measurements for a whole range of frequencies, which would be necessary to completely describe the viscoelastic response, are not presented therein (and not found elsewhere). Nevertheless, by taking the ratio between dynamic and static moduli, we are able to compute a restriction on the free-energy factors β_α^∞, $\alpha = 1, \ldots, m$ (see eqs. (25)).

Before examining this restriction it is necessary to know the deformation state of the coronary artery under the loading conditions (mean inflation pressure of $p_{\mathrm{i}} = 13.33\,(\mathrm{kPa})$) used in the study by GOW & HADFIELD [1979]. Gow and Hadfield stretched the artery until no buckling

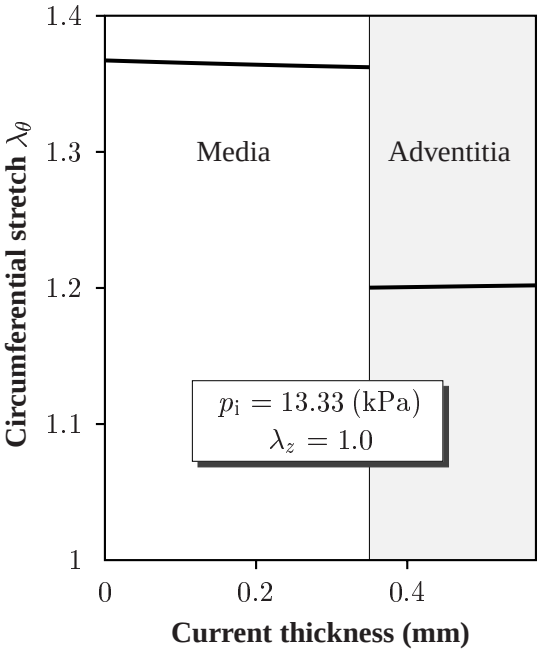

Figure 4: Distribution of the circumferential stretch λ_θ across the coronary arterial wall at internal pressure $p_\mathrm{i} = 13.33\,(\mathrm{kPa})$ and fixed axial stretch $\lambda_z = 1.0$.

occurred during pressurization. No specific axial stretch was given in their paper, so we took the value $\lambda_z = 1.0$. From an (elastic) finite element calculation we may determine the distribution of the circumferential stretch λ_θ across the arterial wall (see Figure 4). As can be seen, λ_θ is nearly uniform across the (current) thickness of the media and adventitia. This result emanates from the consideration of residual stresses (for a discussion see TAKAMIZAWA & HAYASHI [1987], OGDEN & SCHULZE-BAUER [2000], HOLZAPFEL *et al.* [2000]). The stretch λ_θ is discontinuous at the media/adventitia interface which is due to the assumption that the reference configurations of the two layers are independent.

The almost uniform stretch distribution allows us to express the (dynamic) second Piola-Kirchhoff stress in the circumferential direction, say S_dyn, in the simple form

$$S_\mathrm{dyn} = k_\mathrm{M} S_\mathrm{M} + k_\mathrm{A} S_\mathrm{A}, \tag{38}$$

where S_M, S_A are the stresses associated with the media and adventitia, while k_M, k_A are the geometrical ratios of the medial and adventitial thickness with respect to the thickness of the whole arterial wall (the values for our example are $2/3$ and $1/3$, respectively). Note that the stress S_dyn is associated with the dynamic incremental moduli $\mathsf{C}_\mathrm{dyn} = (\partial S_\mathrm{dyn}/\partial\lambda_\theta)/\lambda_\theta$.

Based on the statements of Section 2.1 that viscous effects are attributed mainly to the mechanical behavior of smooth muscle cells, we associate the time-dependent response with the media, which is the heterogeneous arterial layer containing a very large muscle content. By analogy with eq. (18), we may write

$$S_\mathrm{M} = (S^\infty + \sum_{\alpha=1}^{m} Q_\alpha)_\mathrm{M}, \qquad S_\mathrm{A} = S_\mathrm{A}^\infty \tag{39}$$

for the (second Piola-Kirchhoff) stress response in the circumferential direction. Herein the superscript $(\bullet)^\infty$ denotes the elastic stress response of a sufficiently slow process, as $t \to \infty$, while Q_α are non-equilibrium stresses. Note that a sufficiently fast process gives the conditions $Q_{\alpha\,\mathrm{M}} = \beta_\alpha^\infty S_\mathrm{M}^\infty$ for the media (see eq. (26)). Substituting eqs. (39) into (38) and using the initial conditions we obtain

$$S_\mathrm{dyn} = S_\mathrm{stat} + k_\mathrm{M} \sum_{\alpha=1}^{m} \beta_\alpha^\infty S_\mathrm{M}^\infty, \qquad \text{with} \qquad S_\mathrm{stat} = k_\mathrm{M} S_\mathrm{M}^\infty + k_\mathrm{A} S_\mathrm{A}^\infty, \tag{40}$$

where S_stat denotes the (static) second Piola-Kirchhoff stress in the circumferential direction of the arterial wall, i.e. the stress at the equilibrium state. Stress S_stat is associated with the static incremental moduli $\mathsf{C}_\mathrm{stat} = (\partial S_\mathrm{stat}/\partial\lambda_\theta)/\lambda_\theta$. Hence, the ratio of the incremental Young's moduli in the circumferential direction reads

$$\frac{\mathsf{C}_\mathrm{dyn}}{\mathsf{C}_\mathrm{stat}} = \frac{\dfrac{1}{\lambda_\theta}\dfrac{\partial S_\mathrm{dyn}}{\partial \lambda_\theta}}{\dfrac{1}{\lambda_\theta}\dfrac{\partial S_\mathrm{stat}}{\partial \lambda_\theta}} = 1 + \frac{k_\mathrm{M} \displaystyle\sum_{\alpha=1}^{m} \beta_\alpha^\infty}{k_\mathrm{M} + k_\mathrm{A} \dfrac{\mathsf{C}_\mathrm{A}^\infty}{\mathsf{C}_\mathrm{M}^\infty}}, \tag{41}$$

where we used the definitions $\mathsf{C}_\mathrm{M}^\infty = (\partial S_\mathrm{M}^\infty/\partial\lambda_\theta)/\lambda_\theta$ and $\mathsf{C}_\mathrm{A}^\infty = (\partial S_\mathrm{A}^\infty/\partial\lambda_\theta)/\lambda_\theta$ of the (circumferential) elastic stiffness response for the media and adventitia, respectively (as $t \to \infty$). Since the strain states in the media and adventitia are known (see Figure 4), a simple (analytical) calculation gives the ratio $\mathsf{C}_\mathrm{A}^\infty/\mathsf{C}_\mathrm{M}^\infty = 0.36$. Thus, from $(41)_2$, we find that

$$\sum_{\alpha=1}^{m} \beta_\alpha^\infty = 1.57 \tag{42}$$

must hold, which restricts the free-energy factors β_α^∞, $\alpha = 1, \ldots, m$. In order to identify the viscoelastic parameters β_α^∞ and τ_α, $\alpha = 1, \ldots, m$, we need further information.

In the following we make use of the well-established insensitivity of the dissipation of arteries exposed to cyclic loading, as documented by, for example, CHEN & FUNG [1973] and TANAKA & FUNG [1974] using (one-dimensional) extension tests. We aim to model this type of test (performed in the circumferential direction) by means of the proposed viscoelastic (rheological) model (see Section 3.3.1), and to linearize it in the neighborhood of the physiological extension. As a result we obtain a one-dimensional *generalized Maxwell model*, as illustrated in Figure 5(a) (for an extensive discussion see HOLZAPFEL [2000], Section 6.10). This simple model is suitable for representing quantitatively the viscoelastic response of circumferential segments of arteries, as documented in TANAKA & FUNG [1974].

The stiffnesses of the springs (taken as linearly elastic) are determined by Young's moduli $c > 0$ and $c_\alpha > 0$, $\alpha = 1, \ldots, m$. The flow behavior is modeled by a Newtonian viscous fluid responding like a dashpot and specified by the viscosity $\eta_\alpha = c_\alpha \tau_\alpha > 0$, $\alpha = 1, \ldots, m$. For this rheological model the normalized dissipation $\hat{W}_\mathcal{D}$ may be expressed for each cycle as

$$\hat{W}_\mathcal{D} = \pi c \sum_{\alpha=1}^{m} \beta_\alpha^\infty \tau_\alpha |\hat{v}_\alpha^\star| |\hat{u}_\alpha^\star|, \tag{43}$$

$$\text{with} \quad |\hat{v}_\alpha^\star| = \sqrt{\mathrm{Re}(\hat{v}_\alpha^\star)^2 + \mathrm{Im}(\hat{v}_\alpha^\star)^2}, \quad \text{and} \quad |\hat{u}_\alpha^\star| = \sqrt{\mathrm{Re}(\hat{u}_\alpha^\star)^2 + \mathrm{Im}(\hat{u}_\alpha^\star)^2}, \tag{44}$$

Media
$\beta_1^\infty = 0.353\,(-)$
$\tau_1 = 0.001\,(\mathrm{s})$
$\beta_2^\infty = 0.286\,(-)$
$\tau_2 = 0.010\,(\mathrm{s})$
$\beta_3^\infty = 0.298\,(-)$
$\tau_3 = 0.100\,(\mathrm{s})$
$\beta_4^\infty = 0.285\,(-)$
$\tau_4 = 1.000\,(\mathrm{s})$
$\beta_5^\infty = 0.348\,(-)$
$\tau_5 = 10.00\,(\mathrm{s})$

Table 2: Viscoelastic material parameters for the media.

where $\hat{v}_\alpha^\star$ and $\hat{u}_\alpha^\star$ are the normalized complex (internal) velocities and displacements, respectively. For an explicit derivation the reader is referred to the Appendix A.

Finally, we have to specify the Young's modulus $c > 0$ of the free spring, which is required for relation (43). A simple tension test on the media in the circumferential direction allows the stress to be expressed in terms of the circumferential stretch λ_θ (see HOLZAPFEL [2000]). By taking the mean value of the known (physiological) circumferential stretch of the media, which is $\lambda_\theta = 1.36$ (see Figure 4), and the elastic material parameters for the media (see Table 1), it is straightforward to derive the elastic stiffness $c = 634.0\,(\mathrm{kPa})$.

In order to quantify the material parameters we choose a set of five Maxwell elements ($m = 5$) and a set of relaxation times $\tau_1, \ldots, \tau_5$ that cover a time domain of four decades. The free-energy factors $\beta_1, \ldots, \beta_5$ are determined iteratively in such a way that the normalized dissipation $\hat{W}_\mathcal{D}$ is (approximately) constant between frequencies $f = 0.01\,(\mathrm{s}^{-1})$ and $f = 100.0\,(\mathrm{s}^{-1})$. This frequency domain is sufficient for the investigation of physiological loading. By employing eq. (43) and condition (42) we may identify the free-energy factors. As a result of the identification process, the complete set of viscoelastic material parameters for the media are summarized in Table 2.

Figure 5(b) shows a plot of the normalized dissipation $\hat{W}_\mathcal{D}$ versus frequency f based on use of this set of parameters. The solid line denotes the dissipation for the whole rheological model, while each dotted line is associated with a specific Maxwell element. As can be seen, the use of five Maxwell elements gives quite good (constant) dissipation response over four decades. Note that a viscoelastic model based on a single relaxation time, such as can be found in the literature, would never be able to describe the dissipation response of arterial soft tissues under cyclic loading.

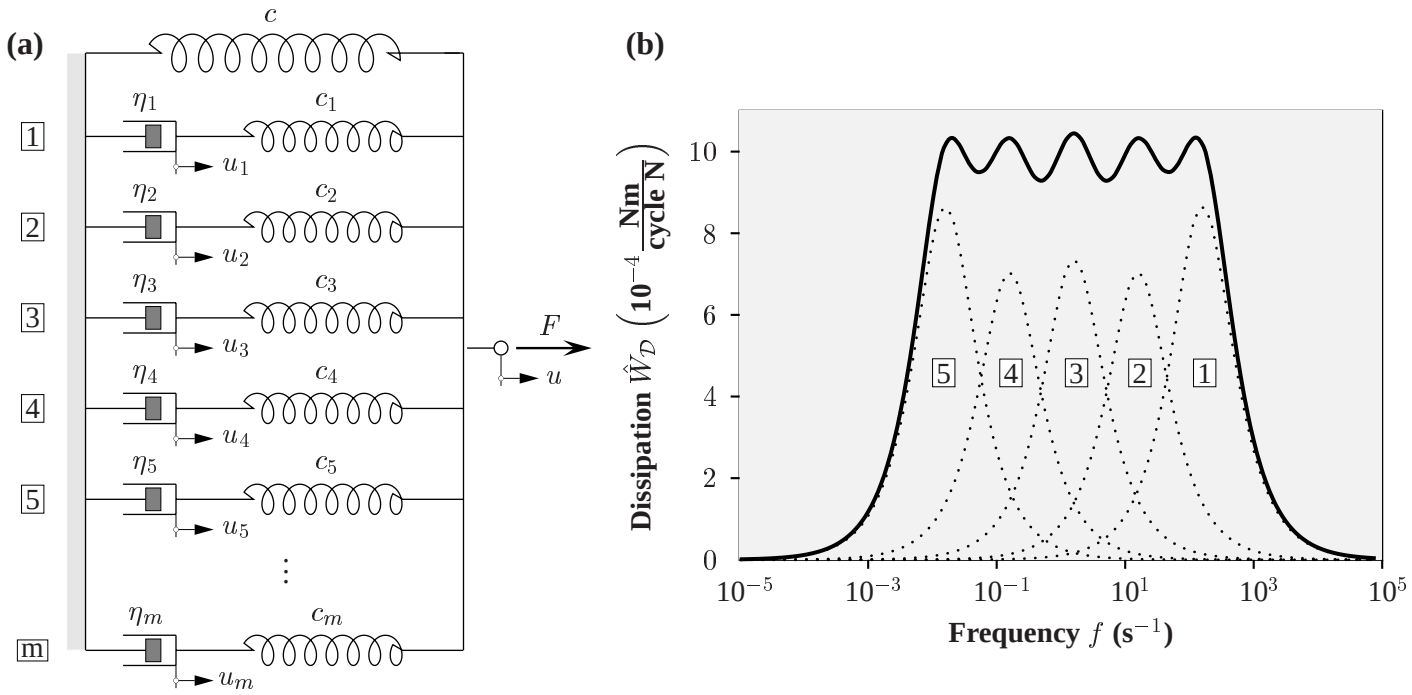

Figure 5: Rheological model for one-dimensional extension tests. (a) Generalized Maxwell model with m Maxwell elements arranged in parallel. (b) Normalized dissipation $\hat{W}_{\mathcal{D}}$ versus frequency f using five Maxwell elements ($m = 5$) and the viscoelastic material parameters for the media according to Table 2. The solid line denotes the dissipation of the whole rheological model, while each dotted line is associated with a specific Maxwell element. Note that $\hat{W}_{\mathcal{D}}$ is (approximately) constant between frequencies $f = 0.01\,(\mathrm{s}^{-1})$ and $f = 100.0\,(\mathrm{s}^{-1})$.

5.2 Viscoelastic behavior of an artery under static and dynamic boundary loadings

Two representative numerical examples investigate the viscoelastic behavior of a healthy and young arterial segment, considered as a two-layer thick-walled tube under static and dynamic boundary loadings. For both examples we take the opened-up geometry of a circular cylindrical tube, as shown in Figure 3, and the elastic and viscoelastic material parameters according to Tables 1 and 2.

In the first example we compare the axial relaxation and creep responses under combined bending, inflation and axial extension of the segment, with (one-dimensional) experimental data of TANAKA & FUNG [1974]. The second example considers the dynamic inflation of the arterial segment subjected to sinusoidal pressure loads. The inner diameter response is investigated in regard to changes in internal pressure and frequency. Sufficiently slow and fast processes, for

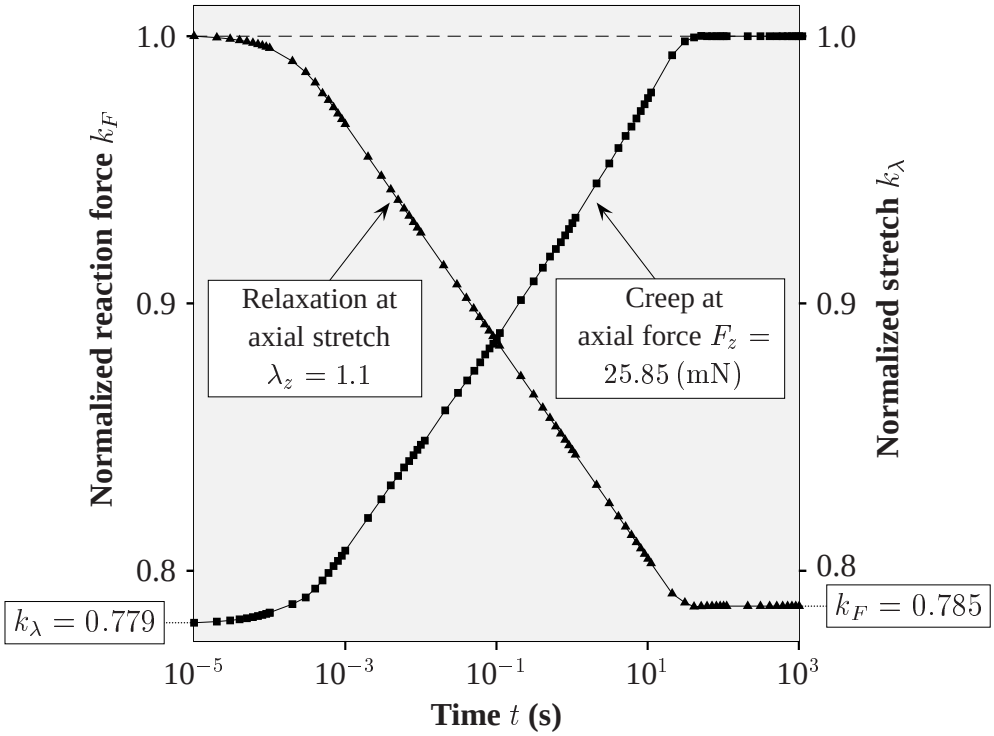

Figure 6: Axial relaxation and creep responses of an arterial segment. Triangles show the relaxation of the normalized axial reaction force $k_F = F_z(\lambda_z, t)/F_z(\lambda_z, 0^+)$ versus time t at axial stretch $\lambda_z = 1.1$. Squares show the creep of the normalized axial stretch $k_\lambda = \lambda_z(F_z, t)/\lambda_z(F_z, 0^+)$ versus time t at axial force $F_z = 25.85\,(\mathrm{mN})$.

which viscous effects are absent, are studied as limiting cases.

5.2.1 Axial relaxation and creep test

We consider the opened-up geometry of a circular cylindrical tube (Figure 3). Bending deformations are applied to the open medial and adventitial sectors to give a closed two-layer thick-walled tube, which is then stretched to $\lambda_z = 1.1$ in the axial direction (simple tension) and fixed subsequently at this elongation. These two processes are performed rapidly so that no time remains for relaxation. Hence, we assume that the relaxation process starts at $t = 0^+$ (for computational reasons we have chosen the deformation period to be $10^{-7}\,(\mathrm{s})$).

Now the axial reaction force, say F_z, is computed as a function of time and normalized with the axial reaction force at $t = 0^+$. Figure 6 shows the relaxation of the normalized axial reaction force, which is denoted by the ratio $k_F = F_z(\lambda_z, t)/F_z(\lambda_z, 0^+)$, versus time t at axial stretch $\lambda_z = 1.1$. The (linear) decrease of k_F is indicated by triangles, while thermodynamic equilibrium (no change in the values of the state variables at any particle of the system) is reached at

$k_F = 0.785$ after some time.

In order to compute the arterial response due to creep, we apply an axial force of $F_z = 25.85\,(\mathrm{mN})$ on the closed tube, which is then kept fixed during the creeping process. By analogy with the above, the viscoelastic process starts at $t = 0^+$. The value of F_z is chosen so that the axial stretch λ_z of the arterial segment is 1.1 at $t = 0^+$, which gives the same initial conditions as in the relaxation test. Now the axial stretch λ_z is computed as a function of time and normalized with $\lambda_z = 1.1$. Figure 6 shows the creep of the normalized axial stretch, which is denoted by the ratio $k_\lambda = \lambda_z(F_z, t)/\lambda_z(F_z, 0^+) = \lambda_z/1.1$, versus time t at axial force $F_z = 25.85\,(\mathrm{mN})$. The (linear) decrease of k_λ is indicated by squares, while thermodynamic equilibrium is reached at $k_\lambda = 0.779$. In comparison with experimental data (see TANAKA & FUNG [1974]) the results given in Figure 6 represent qualitatively the typical viscoelastic behavior of arterial segments.

5.2.2 Dynamic inflation test

The second example investigates the dynamic inflation of the arterial segment of the muscular type under different dynamical loading characteristics. The inner diameter response is investigated in regard to changes in internal pressure and frequency. Sufficiently slow and fast processes, for which viscous effects are absent, are studied as limiting cases.

To achieve a closed two-layer thick-walled tube (pure) bending deformations are applied to the open medial and adventitial sectors. The closed tube is then inflated up to the internal pressure $p_\mathrm{i} = 13.33\,(\mathrm{kPa})$, axially stretched up to $\lambda_z = 1.1$ (simple tension) and then *fixed* at this elongation. We consider a time period of $10^6\,(\mathrm{s})$ in order to compute the equilibrium state of the arterial segment, which we use as the reference state.

Starting from this state we subject the arterial segment to a sinusoidal pressure load $p_\mathrm{i}(t)$ varying between $10.67\,(\mathrm{kPa})$ and $16.0\,(\mathrm{kPa})$ and representing the change of blood pressure between the diastolic and systolic phases. We study load cycles with the specific frequencies of $f_2 = 100.0\,(\mathrm{s}^{-1})$, $f_3 = 1.0\,(\mathrm{s}^{-1})$ and $f_4 = 0.001\,(\mathrm{s}^{-1})$. The evolution of the inner diameter d_i with internal pressure p_i for each of the given frequencies is plotted in Figure 7, and indicated by solid lines. The hysteresis loops demonstrate the typical insensitivity to the frequency over several decades.

As can be seen, the loading and unloading cycles involve about the same dissipation, which is represented by the area between the curves (a measure of the non-recoverable energy). In addition, the deformation responses are stiffer at higher frequencies, a fact which has already been reported by several researchers (see, for example, LEAROYD & TAYLOR [1966] and FUNG [1971]) and which could not be modeled using pseudo-elasticity. Note that the hysteresis is quite small, which is due to the small amplitudes of the pressure loads.

We also investigate sufficiently fast processes, $f_1 \to \infty$, and sufficiently slow processes, $f_5 = 0.0\,(\mathrm{s}^{-1})$ (enough time remains for the arterial segment to adjust itself internally). For computational reasons we have chosen the frequencies to be $f_1 = 10^5\,(\mathrm{s}^{-1})$ and $f_5 = 10^{-5}\,(\mathrm{s}^{-1})$. These two limiting cases describe (reversible) processes during which the arterial segment is in equilibrium at all times and are associated with stiffest and softest responses, respectively.

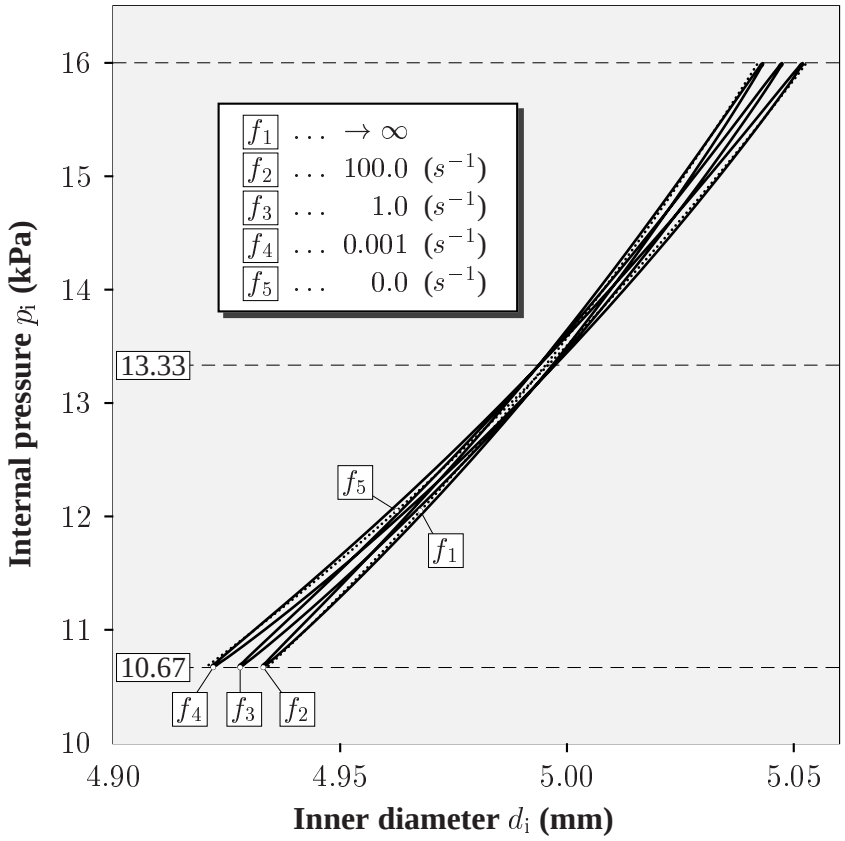

Figure 7: Evolution of the inner diameter d_i of an arterial segment subjected to static and dynamic internal pressure p_i. The solid lines show numerical results based on sinusoidal pressure loads with the frequencies $f_2 = 100.0\,(\mathrm{s}^{-1})$, $f_3 = 1.0\,(\mathrm{s}^{-1})$ and $f_4 = 0.01\,(\mathrm{s}^{-1})$. The dotted curves show numerical results based on the limiting cases $f_1 = 0.0\,(\mathrm{s}^{-1})$ and $f_5 \to \infty$ of the frequencies, representing the stiffest and softest (elastic) responses, respectively.

Viscous effects do not arise and the normalized dissipation $\hat{W}_{\mathcal{D}}$ is zero. The numerical results are plotted in Figure 7 and indicated as dotted curves.

6 Conclusion

In this paper we presented a continuum and numerical setting for a two-layer constitutive model of the viscoelastic three-dimensional stress and deformation response at finite strains, suitable for the *structural* description of healthy young arterial walls in the passive state of the smooth muscles. All constitutive expressions presented are limited to stresses and strains in the *physiological* range. This work is an extension to the viscoelastic regime of a recent paper by HOLZAPFEL *et al.* [2000] dealing with a constitutive framework for the description of the *elastic* response of arterial tissue.

After reviewing arterial histology, particular attention has been paid to incorporating important

histological information in the constitutive model, specifically the orientations of the collagen fibers obtained from a statistical analysis of histological sections from each arterial layer. An algorithmic technique was presented that allows identification of the distribution of the collagen fiber orientations for each arterial layer.

Each solid mechanically relevant layer (media and adventitia) is treated as a fiber-reinforced composite with the fibers corresponding to the collagenous component of the material. The specific constitutive structure for each layer is based on a decomposition of the local stresses into three parts, associated with the volumetric and isochoric *elastic* stress response (responsible for the equilibrium state), and the *viscoelastic* stress response (responsible for the non-equilibrium state). The resulting orthotropic constitutive equation for each layer, given in Lagrangian description, is a function of structural tensors which are the dyadic products of (collagen) fiber directions. Appropriate evolution equations for each of the (isochoric) non-equilibrium stresses and for each constituent of the arterial layer describe the evolution of the viscoelastic process in arteries and guarantee that the hysteresis occurring during a cycling process is relatively insensitive to strain rate over several decades, a crucial mechanical feature of arteries of the muscular type.

On the numerical side, we presented some key aspects, in particular, a three-field functional from which the stationary points were derived. This has led to the nonlinear variational formulation (Euler-Lagrange equations) of the problem in the Lagrangian form, on which the corresponding mixed finite element formulation was based. This approach together with Uzawa's update algorithm has led to a numerically stable solution of the nonlinear boundary-value problem, and is capable of representing the purely isochoric response of arteries by avoiding numerical difficulties such as 'locking' and 'checkerboard' phenomena.

The continuum and numerical formulations have been applied to the structural analysis of a healthy and young arterial segment under various boundary loadings. A proposed identification process of the material parameters provided the necessary set of values. Knowing that the (*in vitro*) residual stress field has a significant effect on the global mechanical behavior and the stress distribution through the deformed arterial walls, we considered the unstressed (and unstrained) configuration of each layer to be an open sector of a thick-walled tube, which is closed by an initial bending to form a load-free (and stressed), circular cylindrical configuration. Two representative examples have been constructed to explore the viscoelastic behavior of a healthy and young muscular arterial segment under static and dynamic boundary loadings within the context of a finite element analysis.

The proposed constitutive framework can be used to study arterial wall mechanics specifically, or, more generally, soft tissue biomechanics, and offers many interesting (but complex) boundary-value problems for investigation. The structural model seems to be sufficiently accurate to warrant its application in the prediction of reliable stress distributions, and is suitable for large scale finite element computation.

Acknowledgements

The authors are indebted to *C.A.J. Schulze-Bauer, MD* from the ‘Computational Biomechanics Group’ in Graz, Austria, for his involvement and ideas, and for valuable discussions. We also would like to thank *P. Regitnig, MD* from the Institute of Pathology for his support in preparing and analyzing the histological sections. Financial support for this research was provided by the *Austrian Science Foundation* under *START-Award Y74-TEC*. This support is gratefully acknowledged.

Appendix A. Derivation of formula (43)

Let $F(t) = F_0 \exp(j\omega t)$ be the (cyclic) force applied to the rheological model illustrated in Figure 5(a), and let u be an external variable which measures the total displacement due to the force. Here F_0 is the amplitude, ω is the angular velocity and j is $\sqrt{-1}$. The (complex) equation of equilibrium for the global system reads,

$$F - cu - \sum_{\alpha=1}^{m}(u - u_\alpha)c_\alpha = 0, \tag{45}$$

where u_α, $\alpha = 1, \ldots, m$, are internal variables, which we interpret as (inelastic) displacements on each dashpot, and $c > 0$ and $c_\alpha = c\beta_\alpha^\infty > 0$, $\alpha = 1, \ldots, m$, denote Young's moduli which characterize the stiffnesses of the associated springs. In addition to eq. (45) we have to fulfill m internal constitutive equations of equilibrium, i.e.

$$(u - u_\alpha)c_\alpha - \eta_\alpha \dot{u}_\alpha = 0, \quad \alpha = 1, \ldots, m, \tag{46}$$

where $\eta_\alpha \dot{u}_\alpha$ is the non-equilibrium stress (internal variable) in the dashpot of the α-Maxwell element characterizing the dissipation mechanism of the viscoelastic model.

Since we are interested in the homogeneous solution of eqs. (45) and (46), we introduce the following *Ansatz* for the displacements, i.e.

$$u = u^\star \exp(j\omega t), \quad u_\alpha = u_\alpha^\star \exp(j\omega t), \quad \alpha = 1, \ldots, m, \tag{47}$$

with the complex values $u^\star$, $u_\alpha^\star$, $\alpha = 1, \ldots, m$, for the displacements. Using eq. (47) and the cyclic loading process $F(t) = F_0 \exp(j\omega t)$, we find from (45) and (46) that

$$F_0 - cu^\star + \sum_{\alpha=1}^{m}(u^\star - u_\alpha^\star)c_\alpha = 0, \quad u_\alpha^\star(c_\alpha + \eta_\alpha j\omega) - c_\alpha u^\star = 0, \quad \alpha = 1, \ldots, m. \tag{48}$$

By means of $(48)_2$, $u_\alpha^\star$ can be substituted into eq. $(48)_1$, which, after some algebraic manipulations, reads

$$\hat{u}^\star = \frac{u^\star}{F_0} = \mathrm{Re}(\hat{u}^\star) + j\mathrm{Im}(\hat{u}^\star), \quad \mathrm{Re}(\hat{u}^\star) = \frac{A}{A^2 + B^2}, \quad \mathrm{Im}(\hat{u}^\star) = \frac{B}{A^2 + B^2}, \tag{49}$$

where $\hat{u}^\star$ denotes the normalized complex displacement of the system and the quantities A and B are given by

$$A = c + \sum_{\alpha=1}^{m} \frac{(\tau_\alpha \omega)^2}{1 + (\tau_\alpha \omega)^2}, \quad B = -\sum_{\alpha=1}^{m} \frac{\tau_\alpha \omega}{1 + (\tau_\alpha \omega)^2}. \tag{50}$$

Expressing $u^\star$ in eq. $(48)_2$ through eq. (49), the normalized complex amount of the internal displacements reads, after some straightforward manipulations,

$$\hat{u}_\alpha^\star = \frac{u_\alpha^\star}{F_0} = \mathrm{Re}(\hat{u}_\alpha^\star) + j\mathrm{Im}(\hat{u}_\alpha^\star), \quad \alpha = 1, \ldots, m, \tag{51}$$

with the real and imaginary parts,

$$\mathrm{Re}(\hat{u}_\alpha^\star) = \frac{A + \tau_\alpha \omega B}{[1 + (\tau_\alpha \omega)^2](A^2 + B^2)}, \quad \mathrm{Im}(\hat{u}_\alpha^\star) = \frac{B - \tau_\alpha \omega A}{[1 + (\tau_\alpha \omega)^2](A^2 + B^2)}, \quad \alpha = 1, \ldots, m. \tag{52}$$

In order to give an analytical expression for the dissipation of the model, we have to derive the normalized complex amount of the internal velocities $\hat{v}_\alpha^\star = \dot{\hat{u}}_\alpha^\star$, $\alpha = 1, \ldots, m$. Using (51) we find that

$$\hat{v}_\alpha^\star = \frac{v_\alpha^\star}{F_0} = \mathrm{Re}(\hat{v}_\alpha^\star) + j\mathrm{Im}(\hat{v}_\alpha^\star), \quad \alpha = 1, \ldots, m, \tag{53}$$

with the real and complex parts

$$\mathrm{Re}(\hat{v}_\alpha^\star) = -\omega \mathrm{Im}(\hat{u}_\alpha^\star), \quad \mathrm{Im}(\hat{v}_\alpha^\star) = \omega \mathrm{Re}(\hat{u}_\alpha^\star). \tag{54}$$

Since displacement and velocity are known for each dashpot, we are able to derive the normalized dissipation $\hat{W}_\mathcal{D}$ of the system for each cycle. By means of the expressions $\mathrm{Re}(\hat{v}_\alpha^\star) = |\hat{v}_\alpha^\star| \cos(\omega t + \pi/2)$ and $\mathrm{Re}(\hat{u}_\alpha^\star) = |\hat{u}_\alpha^\star| \cos(\omega t)$ we find that

$$\hat{W}_\mathcal{D} = \sum_{\alpha=1}^{m} \int_t^{t+\frac{2\pi}{\omega}} \eta_\alpha \mathrm{Re}(\hat{v}_\alpha^\star) \mathrm{Re}(\mathrm{d}\hat{u}_\alpha^\star) = -\sum_{\alpha=1}^{m} \eta_\alpha \omega |\hat{v}_\alpha^\star||\hat{u}_\alpha^\star| \underbrace{\int_t^{t+\frac{2\pi}{\omega}} \cos(\omega\bar{t} + \frac{\pi}{2}) \sin(\omega\bar{t}) \mathrm{d}\bar{t}}_{-\pi/\omega}, \tag{55}$$

$$\text{with} \quad |\hat{u}_\alpha^\star| = \sqrt{\mathrm{Re}(\hat{u}_\alpha^\star)^2 + \mathrm{Im}(\hat{u}_\alpha^\star)^2} \quad \text{and} \quad |\hat{v}_\alpha^\star| = \sqrt{\mathrm{Re}(\hat{v}_\alpha^\star)^2 + \mathrm{Im}(\hat{v}_\alpha^\star)^2}. \tag{56}$$

By using the definition $\tau_\alpha = \eta_\alpha / c_\alpha$ of the relaxation times and $c_\alpha = c\beta_\alpha^\infty$ we obtain from eq. $(55)_2$ the desired result $\hat{W}_\mathcal{D} = \pi c \sum_{\alpha=1}^{m} \beta_\alpha^\infty \tau_\alpha |\hat{v}_\alpha^\star||\hat{u}_\alpha^\star|$.

References

ABÈ, H., HAYASHI, K. & SATO, M. (Eds.) (1996). *Data Book on Mechanical Properties of Living Cells, Tissues, and Organs*. Springer-Verlag. New York.

ARROW, K. J., L. HURWICZ & H. UZAWA (1958). *Studies in Non-Linear Programming*. Stanford University Press. Stanford, CA.

BERGEL, D. H. (1961*a*). 'The dynamic elastic properties of the arterial wall'. *J. Physiol.* **156**, 458–469.

BERGEL, D. H. (1961*b*). 'The static elastic properties of the arterial wall'. *J. Physiol.* **156**, 445–457.

BILLIAR, K. L. & M. S. SACKS (1997). 'A method to quantify the fiber kinematics of planar tissues under biaxial stretch'. *J. Biomech.* **30**, 753–756.

CANHAM, P. B. (1977). 'Orientation of cerebral vascular smooth muscle, mathematically modelled'. *J. Biomech.* **10**, 241–251.

CAREW, T. E., R. N. VAISHNAV & D. J. PATEL (1968). 'Compressibility of the arterial wall'. *Circ. Res.* **23**, 61–68.

CARMINES, D. V., J. H. MCELHANEY & R. STACK (1991). 'A piece-wise non-linear elastic stress expression of human and pig coronary arteries tested *in vitro*'. *J. Biomech.* **24**, 899–906.

CHEN, Y. L. & Y. C. FUNG (1973). Stress-history relations of rabbit mesentery in simple elongation. In 'ASME 1973 Biomechanics Symposium, AMD-Vol. 2'. American Society of Mechanical Engineers. New York. pp. 9–10.

CHUONG, C. J. & Y. C. FUNG (1986). Residual stress in arteries. In G. W. SCHMID-SCHÖNBEIN, S. L.-Y. WOO & B. W. ZWEIFACH (Eds.). 'Frontiers in Biomechanics'. Springer-Verlag. New York. pp. 117–129.

CLARK, J. M. & S. GLAGOV (1985). 'Transmural organization of the arterial media: The lamellar unit revisited'. *Arteriosclerosis* **5**, 19–34.

COLEMAN, B. D. & M. E. GURTIN (1967). 'Thermodynamics with internal state variables'. *J. Chem. Phys.* **47**, 597–613.

COLEMAN, B. D. & W. NOLL (1963). 'The thermodynamics of elastic materials with heat conduction and viscosity'. *Arch. Rational Mech. Anal.* **13**, 167–178.

COPE, D. A. & M. R. ROACH (1975). 'A scanning electron microscopy study of human cerebral arteries'. *Canad. J. Physiol. Pharm.* **53**, 651–659.

DOBRIN, P. B. (1999). 'Distribution of lamellar deformations. implications for properties of the arterial media'. *Hypertension* **33**, 806–810.

FERDMAN, A. G. & I. V. YANNAS (1993). 'Scattering of light from histologic sections: A new method for the analysis of connective tissue'. *J. Invest. Dermatol.* **100**, 710–716.

FINLAY, H. M., P. WHITTAKER & P. B. CANHAM (1998). 'Collagen organization in the branching region of human brain arteries'. *Stroke* **29**, 1595–1601.

FLORY, P. J. (1961). 'Thermodynamic relations for highly elastic materials'. *Trans. Faraday Soc.* **57**, 829–838.

FUNG, Y. C. (1971). Stress-strain-history relations of soft tissues in simple elongation. In Y. C. FUNG, N. PERRONE & M. ANLIKER (Eds.). 'Biomechanics: Its Foundations and Objectives'. Prentice-Hall, Inc., Englewood Cliffs. New Jersey. pp. 181–208. Chapter 7.

FUNG, Y. C. (1980). On pseudo-elasticity of living tissues. In S. NEMAT-NASSER (Ed.). 'Mechanics Today'. Pergamon Press. Oxford.

FUNG, Y. C. (1993). *Biomechanics. Mechanical Properties of Living Tissues*. 2nd edn. Springer-Verlag. New York.

FUNG, Y. C., K. FRONEK & P. PATITUCCI (1979). 'Pseudoelasticity of arteries and the choice of its mathematical expression'. *Am. J. Physiol.* **237**, H620–H631.

GASSER, T. C. & G. A. HOLZAPFEL (2001). 'A rate-independent elastoplastic constitutive model for fiber-reinforced composites at finite strains: Continuum basis, algorithmic formulation and finite element implementation'. submitted.

GOW, B. S. & C. D. HADFIELD (1979). 'The elasticity of canine and human coronary arteries with reference to postmortem changes'. *Circ. Res.* **45**, 588–594.

HAYASHI, K. (1993). 'Experimental approaches on measuring the mechanical properties and constitutive laws of arterial walls'. *J. Biomech. Engr.* **115**, 481–488.

HOLZAPFEL, G. A. (2000). *Nonlinear Solid Mechanics. A Continuum Approach for Engineering*. John Wiley & Sons. Chichester.

HOLZAPFEL, G. A. & J. C. SIMO (1996). 'Entropy elasticity of isotropic rubber-like solids at finite strains'. *Comput. Meth. Appl. Mech. Engr.* **132**, 17–44.

HOLZAPFEL, G. A. & T. C. GASSER (2001). 'A viscoelastic model for fiber-reinforced composites at finite strains: Continuum basis, computational aspects and applications'. *Comput. Meth. Appl. Mech. Engr.* **190**, 4379–4403.

HOLZAPFEL, G. A., T. C. GASSER & R. W. OGDEN (2000). 'A new constitutive framework for arterial wall mechanics and a comparative study of material models'. *J. Elasticity* **61**, 1–48.

HUGHES, T. J. R. (2000). *The Finite Element Method: Linear Static and Dynamic Finite Element Analysis*. Dover. New York.

HUMPHREY, J. D. (1995). 'Mechanics of the arterial wall: Review and directions'. *Critical Reviews in Biomed. Engr.* **23**, 1–162.

LANGEWOUTERS, G. J., K. H. WESSELING & W. J. A. GOEDHARD (1984). 'The static elastic properties of 45 human thoracic and 20 abdominal aortas *in vitro* and the parameters of a new model'. *J. Biomech.* **17**, 425–435.

LEAROYD, B. M. & M. G. TAYLOR (1966). 'Alterations with age in the viscoelastic properties of human arterial walls'. *Circ. Res.* **18**, 278–292.

LUBLINER, J. (1990). *Plasticity Theory*. Macmillan Publishing Company. New York.

MARSDEN, J. E. & T. J. R. HUGHES (1994). *Mathematical Foundations of Elasticity*. Dover. New York.

MIEHE, C. (1996). 'Numerical computation of algorithmic (consistent) tangent moduli in large-strain computational inelasticity'. *Comput. Meth. Appl. Mech. Engr.* **134**, 223–240.

NAGTEGAAL, J. C., D. M. PARKS & J. R. RICE (1974). 'On numerically accurate finite element solutions in the fully plastic range'. *Comput. Meth. Appl. Mech. Engr.* **4**, 153–177.

NICHOLS, W. W. & M. F. O'ROURKE (1998). *McDonald's Blood Flow in Arteries*. 4th edn. Arnold. London. chapter 4, pp. 73–97.

OGDEN, R. W. (1978). 'Nearly isochoric elastic deformations: Application to rubberlike solids'. *J. Mech. Phys. Solids* **26**, 37–57.

OGDEN, R. W. & C. A. J. SCHULZE-BAUER (2000). Phenomenological and structural aspects of the mechanical response of arteries. In J. CASEY & G. BAO (Eds.). 'Mechanics in Biology'. The American Society of Mechanical Engineers (ASME). New York. AMD-Vol. 242/BED-Vol. 46, pp. 125-140.

PATEL, D. J. & D. L. FRY (1969). 'The elastic symmetry of arterial segments in dogs'. *Circ. Res.* **24**, 1–8.

PETERS, M. W., P. B. CANHAM & H. M. FINLAY (1983). 'Circumferential alignment of muscle cells in the tunica media of the human brain artery'. *Blood Vessels* **20**, 221–233.

RANVIER, L. (1880). 'Leçons d'anatomie générale sur le système musculaire'. *Progrès médical, Delahaye.*

RHODIN, J. A. G. (1962). 'Fine structure of vascular walls in mammals, with special reference to smooth muscle component'. *Physiol. Rev.* **42**, 48–81.

RHODIN, J. A. G. (1967). 'The ultrastructure of mammalian arterioles and precapillary sphincters'. *J. Ultrastruct. Res.* **18**, 181–223.

RHODIN, J. A. G. (1980). Architecture of the vessel wall. In D. F. BOHR, A. D. SOMLYO & H. V. SPARKS (Eds.). 'Handbook of Physiology, The Cardiovascular System'. Vol. 2. American Physiologial Society. Bethesda, Maryland. pp. 1–31.

ROACH, M. R. & A. C. BURTON (1957). 'The reason for the shape of the distensibility curve of arteries'. *Canad. J. Biochem. Physiol.* **35**, 681–690.

ROY, C. S. (1880-82). 'The elastic properties of the arterial wall'. *J. Physiol.* **3**, 125–159.

SCHULZE-BAUER, C. A. J., P. REGITNIG & G.A. HOLZAPFEL (2001). 'Mechanics of the human femoral adventitia including high-pressure response'. *Am. J. Physiol.* in press.

SILVER, F. H., D. L. CHRISTIANSEN & C. M. BUNTIN (1989). 'Mechanical properties of the aorta: A review'. *Critical Reviews in Biomed. Engr.* **17**, 323–358.

SIMO, J. C. (1987). 'On a fully three-dimensional finite-strain viscoelastic damage model: Formulation and computational aspects'. *Comput. Meth. Appl. Mech. Engr.* **60**, 153–173.

SIMO, J. C. & C. MIEHE (1992). 'Associative coupled thermoplasticity at finite strains: Formulation, numerical analysis and implementation'. *Comput. Meth. Appl. Mech. Engr.* **98**, 41–104.

SIMO, J. C. & R. L. TAYLOR (1991). 'Quasi-incompressible finite elasticity in principal stretches. Continuum basis and numerical algorithms'. *Comput. Meth. Appl. Mech. Engr.* **85**, 273–310.

SIMO, J. C., R. L. TAYLOR & K. S. PISTER (1985). 'Variational and projection methods for the volume constraint in finite deformation elasto-plasticity'. *Comput. Meth. Appl. Mech. Engr.* **51**, 177–208.

SIMO, J. C. & T. J. R. HUGHES (1998). *Computational Inelasticity*. Springer-Verlag. New York.

SOMLYO, A. P. & A. V. SOMLYO (1968). 'Vascular smooth muscle. i: Normal structure, pathology, biochemistry and biophysics'. *Physiol. Rev.* **20**, 197–272.

SPENCER, A. J. M. (1984). Constitutive theory for strongly anisotropic solids. In A. J. M. SPENCER (Ed.). 'Continuum Theory of the Mechanics of Fibre-Reinforced Composites'. Springer-Verlag. Wien. pp. 1–32. CISM Courses and Lectures No. 282, International Centre for Mechanical Sciences.

STRONG, K. C. (1938). 'A study of the structure of the media of the distributing arteries by the method of microdissection'. *Anat. Rec.* **72**, 151–168.

TAKAMIZAWA, K. & K. HAYASHI (1987). 'Strain energy density function and uniform strain hypothesis for arterial mechanics'. *J. Biomech.* **20**, 7–17.

TANAKA, T. T. & Y. C. FUNG (1974). 'Elastic and inelastic properties of the canine aorta and their variation along the aortic tree'. *J. Biomech.* **7**, 357–370.

TAYLOR, R. L. (2000). *FEAP – A Finite Element Analysis Program - Version 7.3*. University of California at Berkeley.

TODD, M. E., C. G. LAYE & D. N. OSBORNE (1983). 'The dimensional characteristics of smooth muscle in rat blood vessels: A computer-assisted analysis'. *Circ. Res.* **53**, 319–331.

VAISHNAV, R. N. & J. VOSSOUGHI (1983). Estimation of residual strains in aortic segments. In C. W. HALL (Ed.). 'Biomedical Engineering II: Recent Developments'. Pergamon Press. New York. pp. 330–333.

VALANIS, K. C. (1972). *Irreversible Thermodynamics of Continuous Media, Internal Variable Theory*. Springer-Verlag. Wien.

VOSSOUGHI, J. (1992). Longitudinal residual strains in arteries. In 'Proceedings of the 11th Southern Biomedical Engineering Conference'. Memphis, TN. October 2-4, 1992, pp. 17-19.

WALMSLEY, J. G. & P. B. CANHAM (1979). 'Orientation of nuclei as indicators of smooth muscle cell alignment in the cerebral artery'. *Blood Vessels* **16**, 43–51.

WEISS, J. A., B. N. MAKER & S. GOVINDJEE (1996). 'Finite element implementation of incompressible, transversely isotropic hyperelasticity'. *Comput. Meth. Appl. Mech. Engr.* **135**, 107–128.

WERTHEIM, M. G. (1847). 'Mémoire sur l'élasticité et la cohésion des principaux tissus du corps humain'. *Annales de Chimie et de Physique* **21**, 385–414.

WOLINSKY, H. & S. GLAGOV (1964). 'Structural basis for the static mechanical properties of the aortic media'. *Circ. Res.* **14**, 400–413.

WOLINSKY, H. & S. GLAGOV (1967). 'A lamellar unit of aortic medial structure and function in mammals'. *Circ. Res.* **20**, 90–111.

WOO, S. L. Y., B. R. SIMON, S. C. KUEI & W. H. AKESON (1979). 'Quasi-linear viscoelastic properties of normal articular cartilage'. *J. Biomech. Engr.* **102**, 85–90.

XIE, J., J. ZHOU & Y. C. FUNG (1995). 'Bending of blood vessel wall: Stress-strain laws of the intima-media and adventitia layers'. *J. Biomech. Engr.* **117**, 136–145.